RESEARCH REPORT

VTT-R-05722-09

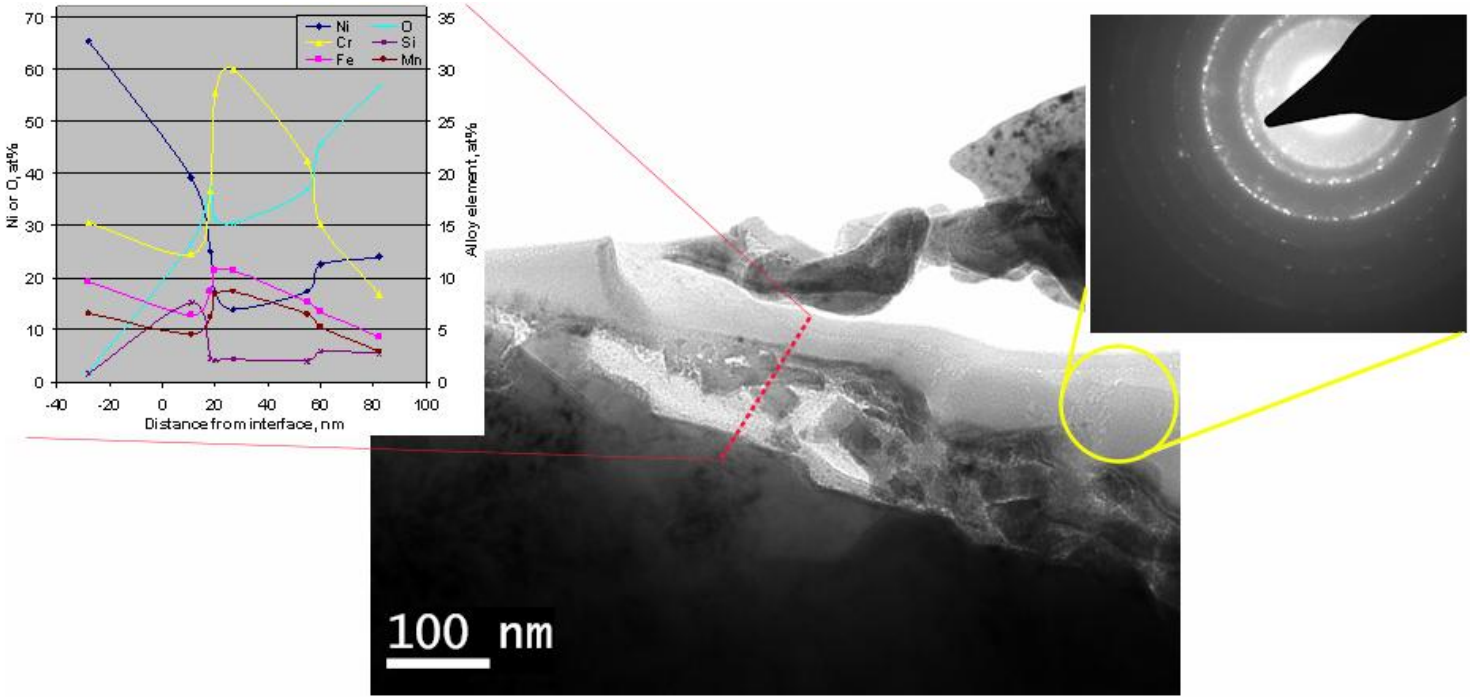

TEM investigation of cracks in dissimilar metal weld Inconel 182 following doped steam testing

Authors: Wade Karlsen, Janne Pakarinen

Confidentiality: Public

Report's title

TEM investigation of cracks in dissimilar metal weld Inconel 182 following doped steam testing

Customer, contact person, address	Order reference
Teollisuuden Voima Oy, Neste Jacobs Oy,Metso Materials Technology, Posiva, Fortum Nuclear Services, STUK, TKK	
Project name	**Project number/Short name**
Performance and Aging of Dissimilar Metal Joints	12420/PERDI
Author(s)	**Pages**
Wade Karlsen, Janne Pakarinen	29/64
Keywords	**Report identification code**
TEM, EAC, Alloy 182, doped steam, oxide	VTT-R-05722-09

Summary

This study examined the oxide compositions and structures found in cracks produced in a four-point bend test bar that was exposed to an environment of steam doped with Cl, F and S ions at 400°C. Three different example cracks were extracted from the test bar, two from near the tips of deep cracks (Cracks A and C), and one shallow, surface crack (Crack B). EDS and SAD results indicated that two main kinds of oxides were present, containing mostly nickel, but arranged as a 30-50 nm wide Cr- and Fe-rich inner layer showing spinel structure, and an outer layer having NiO type structure filling the rest of the crack. A significant amount of Cl as well as some F and S were detected in the oxide of the surface crack. Based on the observation of an epitaxial relation between the NiO and the matrix, as well as the relative thicknesses and composition variations in the different oxide layers, it would seem that the dopants served to initiate the crack, and then once initiated, the formation of the NiO was dominant. The Cr-rich spinel inner layer then subsequently grew at the interface with the matrix, becoming thicker and more Cr- and Fe-rich as it evolved, perhaps promoting the transport of Ni metal ions towards the outer oxide surface. Such behaviour is counter to that typically expected for PWR environments, but at this moment the real conditions existing in the crack during doped steam testing are unknown, so the drivers of the crack oxide evolution in doped steam are not self-evident. This summary report is focused on the results analysis and discussion. More results and documentation of the characterization are presented in the Finnish-language Appendix to this report.

Confidentiality	Public

Espoo, 4.11.2009

Written by	Reviewed by	Accepted by
Wade Karlsen Senior Research Scientist	Pertti Aaltonen Senior Research Scientist	Pentti Kauppinen Technology Manager

VTT's contact address

Kemistintie 3, Espoo; P.O. Box 1000, FI-02044 VTT, FINLAND

Distribution (customer and VTT)

Teollisuuden Voima Oy, Neste Jacobs Oy,Metso Materials Technology, Posiva, Fortum Nuclear Services, STUK, TKK, VTT archive

Contents

1 Introduction

Maintaining the structural integrity of key components of nuclear power plants (NPP) throughout their service life is essential for plant safety and availability. The operating experience of major NPP pressure boundary components has shown that dissimilar metal weld joints can jeopardize the plant availability and safety because of increased incidences of environment-assisted cracking (EAC, PWSCC) of Alloy 600 and its corresponding weld metals (Alloys 182/82). Alloy 690 and associated weld metals (Alloys 152/52) are often used for repair and replacement of the affected thick-section components. The ERIPARI project examined the susceptibility of these alloys to hot cracking as well as their PWSCC susceptibility in reactor primary water. The selection of these new materials relies mainly on excellent laboratory results and short-term service experience, but their long-term behaviour and performance in the plant has still to be demonstrated. By examining the cracking behaviour of tested materials though, some insight may be gained that can enable better prediction of the performance to be expected over the long term, particularly of the new alloy solutions. Such an effort has been continued in the current PERDI project.

The dissimilar metal welds studied in the ERIPARI and PERDI projects have shown clear segregation of Nb, Si, P and Mn in the final portion of liquid solidifying at dendrite boundaries. Hot cracking was found to occur along the dendrite boundaries. The susceptibility to hot cracking in the weld mock-up samples was observed to follow the order Alloy 152 > Alloy 52 > Alloy 182 > Alloy 82, while in pure (undiluted) weld metal hot cracking tests the susceptibility followed the order: Alloy 182 ≥ Alloy 152 > Alloy 52 ≥ Alloy 82. The differences are thought to be related to dilution effects in mock-up welds, because Fe, Si, and C promote the eutectic phases, expanding the solidification temperature range [1]. However, of particular interest in the continuation PERDI project, is the possible role of the hot-crack susceptibility in promoting subsequent EAC cracking.

EAC tests on nickel-based alloys in general tend to be much longer, and therefore more resource intensive, than similar tests on austenitic stainless steels. Thus, a limited amount of laboratory EAC test results is available for the material combinations of dissimilar metal welds of nuclear power plants, particular of the newer, more resistant combinations. As crack initiation takes a very long time in actual LWR water at relevant operating temperatures (years or decades), accelerated tests have been conducted in an environment consisting of hydrogenated 400°C steam doped with fluoride, chloride and sulphate anions. In the ERIPARI project, comparison tests were performed on the material combinations in similar doped-steam conditions, utilizing bolt-loaded four-point bend specimens.

In the current study within the PERDI project, TEM examinations were carried out on cracks which were formed in one of the Alloy 600/182 material combinations during the doped-steam test. Previous work examined the hot-cracks formed in the same material combination.

2 Materials and Methods

The material of this study came from the ERIPARI doped steam four-point-bend test series on the materials combination “Mock-up TV.” Mock-up TV4 was comprised of Alloy 182 weld metal joining an Alloy 600 and the 182-butter of stainless steel clad pressure vessel steel, in the geometrical combination shown in Figure 1. The nominal composition of the weld metal (wt%) is 68 Ni, 16 Cr, 6.7 Fe, 6.5 Mn, 1.8 Nb, 0.8 Si. The specimen production, heat-treatment and subsequent doped-steam four-point-bend testing are all described in Section 3 of the ERIPARI report published as VTT Research Notes 2399. For context, the reader is encouraged to review that chapter.

The TEM examinations were carried out on cracks extracted from the four-point-bend specimen TV4-7, which (according to Tables 3.1 and 3.2 of the aforementioned report) contained a longitudinally-oriented weld loaded with 1% of strain, and exposed to four autoclave cycles for a total exposure time of 1172.5 hours. The first cracks had been found (by the dye penetrant method) after about 734.5 hours of exposure. By test end the number of cracks was greater than ten, located in the Alloy 600 base, the 182 weld and the 182 butter regions of the specimen, and reached a maximum length of about 4 mm. The cracking occurred across the weld, perpendicular to the weld (and specimen) axis. Noteworthy is that its pair (TV4-8) did not appear to contain any cracks, even by the end of the fourth exposure, while similar weld orientations of the same material combination but loaded at the lower strain level of 0.35%, *did* exhibit cracks in dye penetrant examinations.

Extraction and successful TEM characterisation of cracks and crack tips requires careful attention to the specimen (foil) preparation. Particular cracks of interest for TEM examination were first identified by preparing a metallographic cross section of the cracked four-point-bend test bar, in the longitudinal orientation (e.g. perpendicular to the cracks). Prior to this though, the cracks in the as-received four-point-bend specimen were first vacuum back-filled with very low-viscosity M-Bond epoxy, to help preserve the oxides. Coarse grinding of the cross-section was then used to remove the Alloy 600 base material residing on one side of the weld, to reach the crack-containing Alloy 182 of interest. This was followed by standard metallographic grinding on wet SiC papers, followed by fine polishing with diamond paste on a fabric platen.

In the polished cross-section it was observed that many more cracks were present in TV4-7 than originally evident based only on the dye-penetrant inspections, with some appearing to not necessarily even emerge at the specimen surface (thereby preventing detection by dye-penetrant methods). Therefore, a similar metallographic section was prepared from four-point-bend bar TV4-8, which had not exhibited cracks in dye-penetrant inspections. However, no cracks were found in that specimen by metallography either, so no further examinations were carried out on that material.

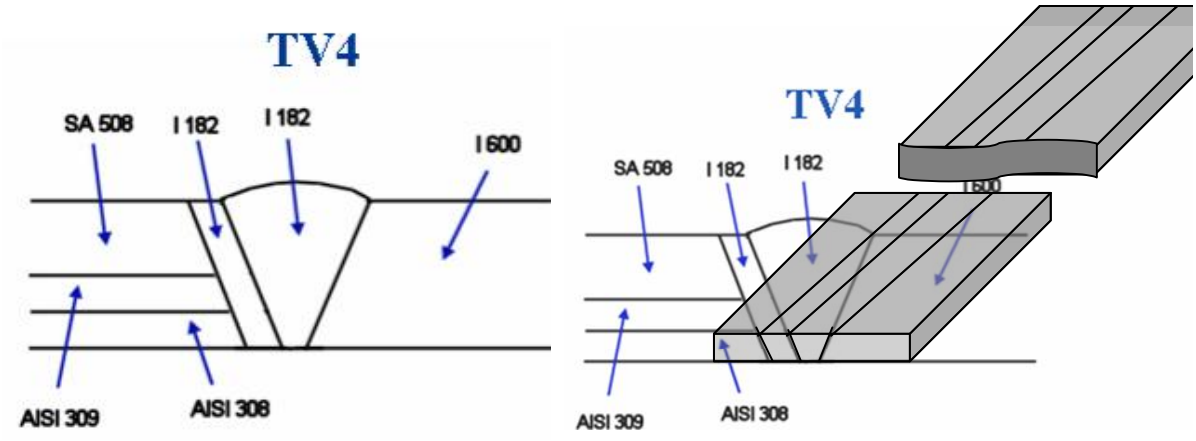

Figure 1: Geometry of dissimilar weld TV4 (left) and a schematic of the region from which the longitudinally-oriented four-point bend specimens were extracted at the weld root.

Because individual cracks in TV4-7 spanned the width of the weld to greater or lesser degree, it was deemed important to more accurately determine their geometry to facilitate locating TEM specimens. Therefore, the cross-section specimen was de-mounted and then the weld face was ground and polished by hand. This enabled both a cross-section (depth) and a length estimate for the cracks of interest.

Several different kinds of cracks were chosen for TEM examination, sampling both shallow surface cracks, as well as deeply-penetrating multi-branched cracks. Once a crack region of interest was identified, a 5 mm wide strip of material containing the crack (or generally several cracks) was cut from the piece with a water-cooled high-speed micro saw, perpendicular to the weld direction (and thus parallel to the crack orientation.) This produced a piece about 5 x 8 x 3 mm in size, as shown in Figure 2. Each of these blocks was labelled with an integer added to the four-point-bend specimen identifier, as TV4-7-1, TV4-7-2, etc.

A number of cross-section TEM blanks about 0.5 mm thick were then sliced from each block, perpendicular to the crack length, as illustrated in Figure 2. In that image the main crack of interest is visible within the oval. Each resulting blank was identified by an integer added to the block label, e.g. TV4-7-4-1, TV4-7-4-2, etc.

In order to target particular regions and to preserve the integrity of the oxides within the cracks, cross-section specimens of the oxide-filled cracks were fabricated by a process of mechanical thinning of the blanks, avoiding conventional electrolytic techniques. Numerous “working images” were used to document the specimen preparation process, and many of those are included in the Appendix. The slice of the region of interest was first ground down to about 0.1 mm thick, and then trimmed to the appropriate 3 mm size to fit the TEM specimen holder. A Gatan Dimpler was then used to gently grind and polish a small dimple in one side of the specimen, targeting the region of interest (generally the crack tip). This was followed by ion milling to electron transparency. As detailed in the Appendix, several different methods were tried in the dimpling process. However, the process of final polishing with aluminium oxide was abandoned after the first specimen series, when it was discovered that residual aluminium (and presumably oxygen) subsequently showed up in analytical measurements.

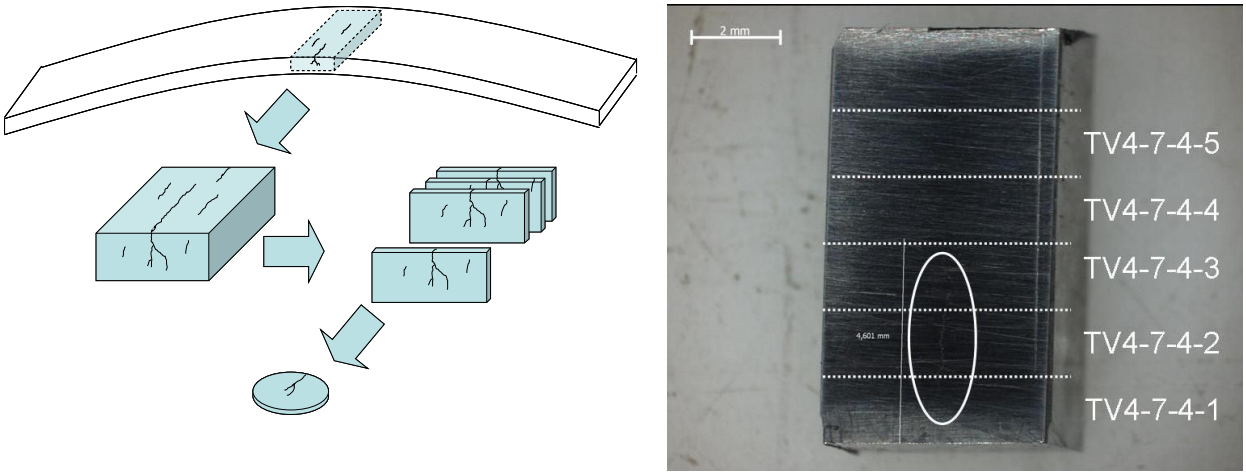

Figure 2: Schematic of specimen blank extraction process from four-point bend specimen (left) and example of the slicing of a crack-containing block (top view) into a series of TEM specimen blanks. The main crack of interest in TV4-7-4 was located in the middle (circled).

TEM examinations were carried out with a CM200 STEM equipped with a field-emission gun (FEG) source. Selected area electron diffraction (SAD) was combined with energy dispersive x-ray spectroscopy (EDS) in order to identify the composition and structure of the oxides filling the cracks.

3 Results

There were three main kinds of cracks found in the materials examined. The most common and of greatest interest were the deep, branching, irregular cracks like that shown at low magnification in the light micrograph and SEM backscatter electron (BSE) images of Figure 3 and Figure 4, respectively. Occasionally the cracks left the plane of the cross-section, re-emerging elsewhere. Also found were a few examples of what appear to be tearing-type cracks, as shown in Figure 5, and at higher magnification in Figure 6. Finally, there were many short cracks evident at the weld surface, as shown in Figure 7. Perhaps actually a subset of the deep, branching cracks, they appeared to extend from what may have been pits or grooves at the surface. The image in Figure 8 shows a typical deep, branched EAC crack formed in the TV4-7 doped-steam four-point-bend test. The crack path suggests that it follows the dendrite boundaries of the weld metal. In BSE imaging higher atomic number atoms tend to appear lighter, so the light particles visible in both Figure 4 and Figure 8 are probably the primary niobium carbides that were also observed in the as-welded materials. As shown at higher magnification in Figure 9, the branched cracks are filled with some material, probably oxide, all the way to the tips. The tips themselves are quite tight. The method of mechanical grinding, dimpling and ion milling produces TEM specimens that have only limited electron transparency within the metal, while the oxides are generally readily visible. Thus, the characterization efforts in this study were devoted primarily to the identification and spatial analysis of the oxides within the cracks.

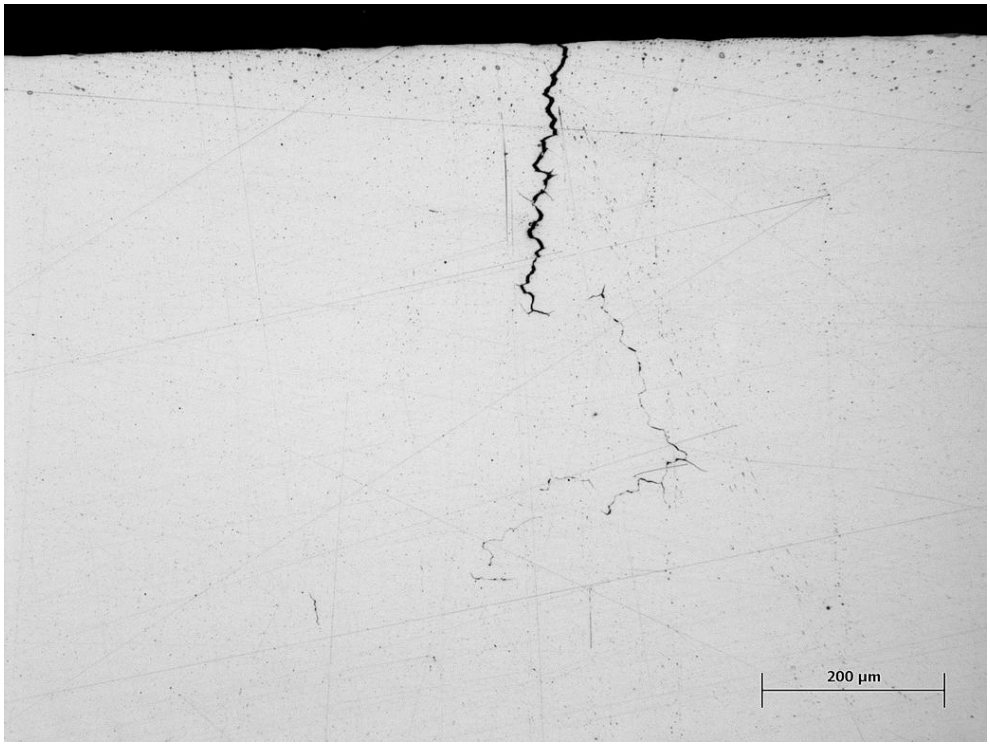

Figure 3: Light micrograph of a deep, wandering crack in four-point-bend specimen TV4-7 following the exposure to doped steam. While the specimen exhibited several of such large cracks open at the mouth, many more were very much tighter and even more branched.

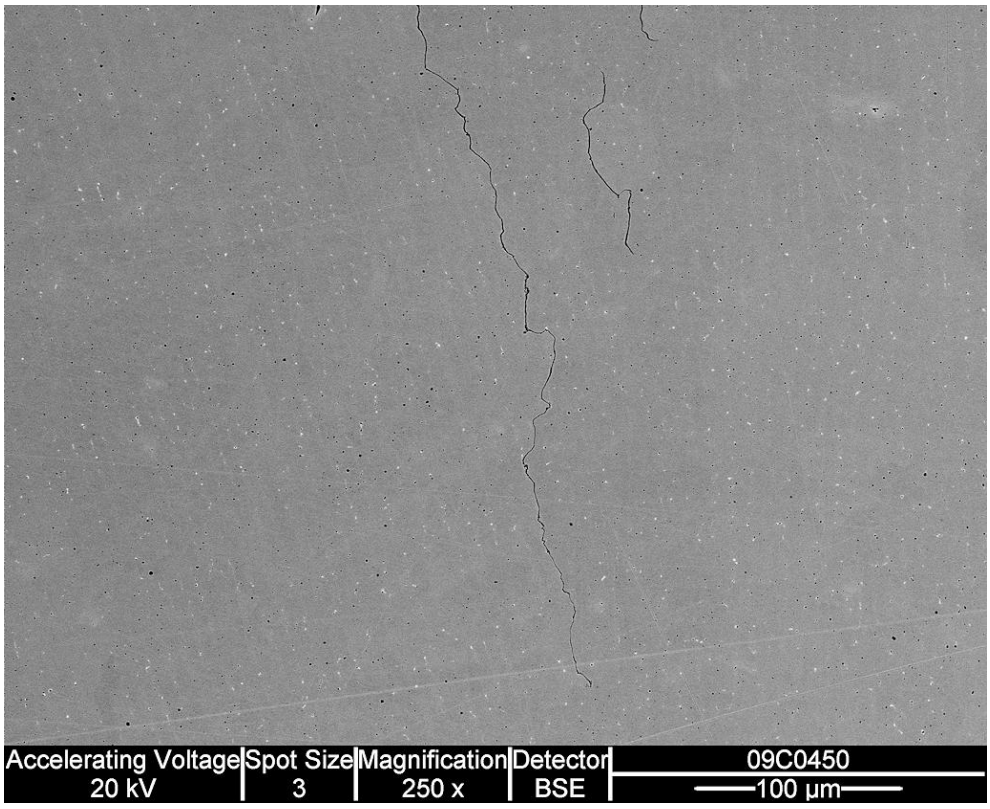

Figure 4: SEM backscatter electron (BSE) image of a typical EAC crack found in four-point-bend specimen TV4-7 following the exposure to doped steam. The light particles are probably Nb-carbides.

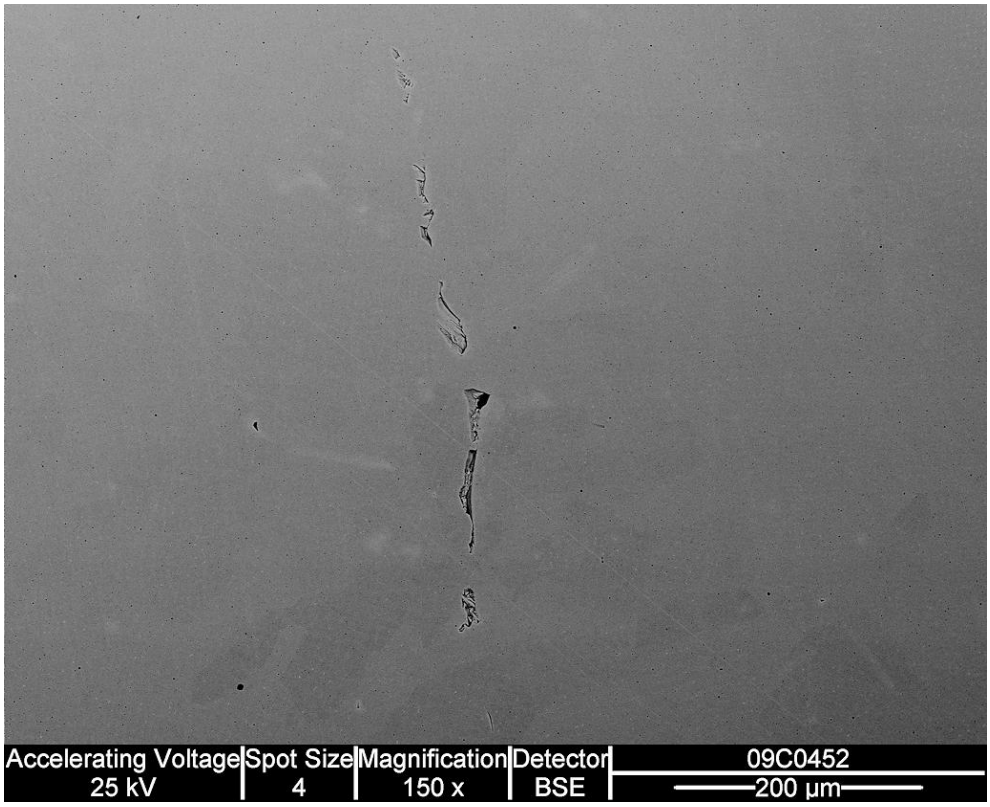

Figure 5: SEM BSE image of what would appear to be a tearing-type crack found in four-point-bend specimen TV4-7 following the exposure to doped steam.

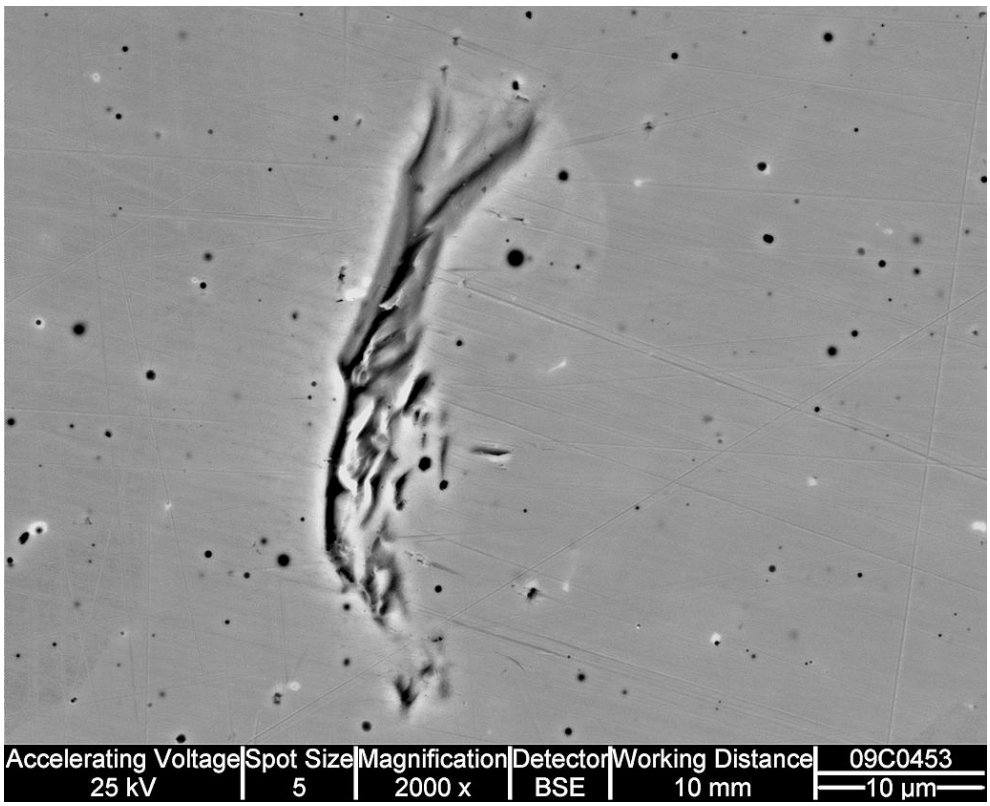

Figure 6: Higher magnification SEM BSE image of a tearing-type crack found in four-point-bend specimen TV4-7 following the exposure to doped steam.

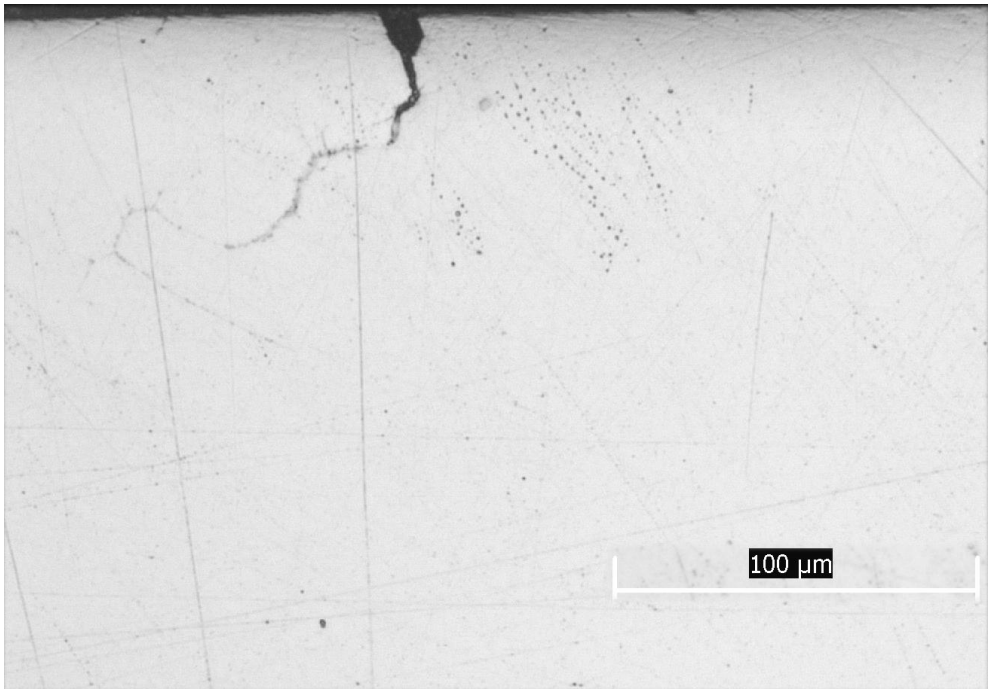

Figure 7: At the weld surface, many small cracks appeared to extend from pits or grooves at the surface, as shown in this light micrograph. It is filled with what is probably oxide.

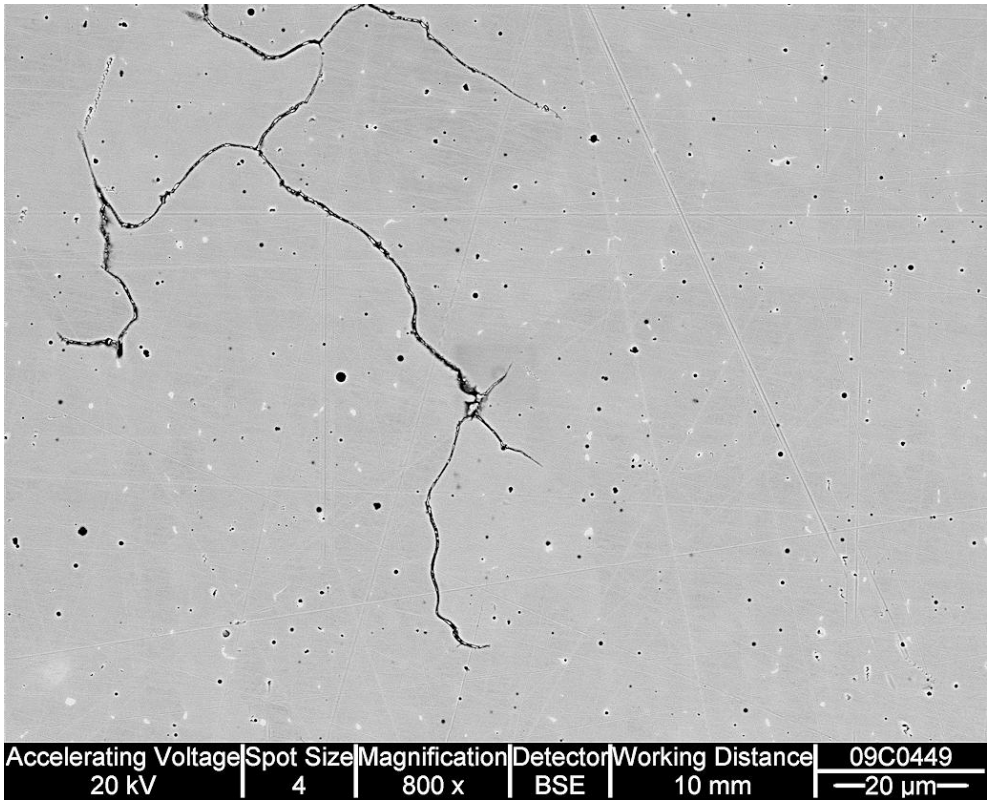

Figure 8: Higher magnification SEM BSE image of a deep crack. They tended to be heavily branched, perhaps following the solidification dendrite boundaries. The light particles are probably niobium carbides.

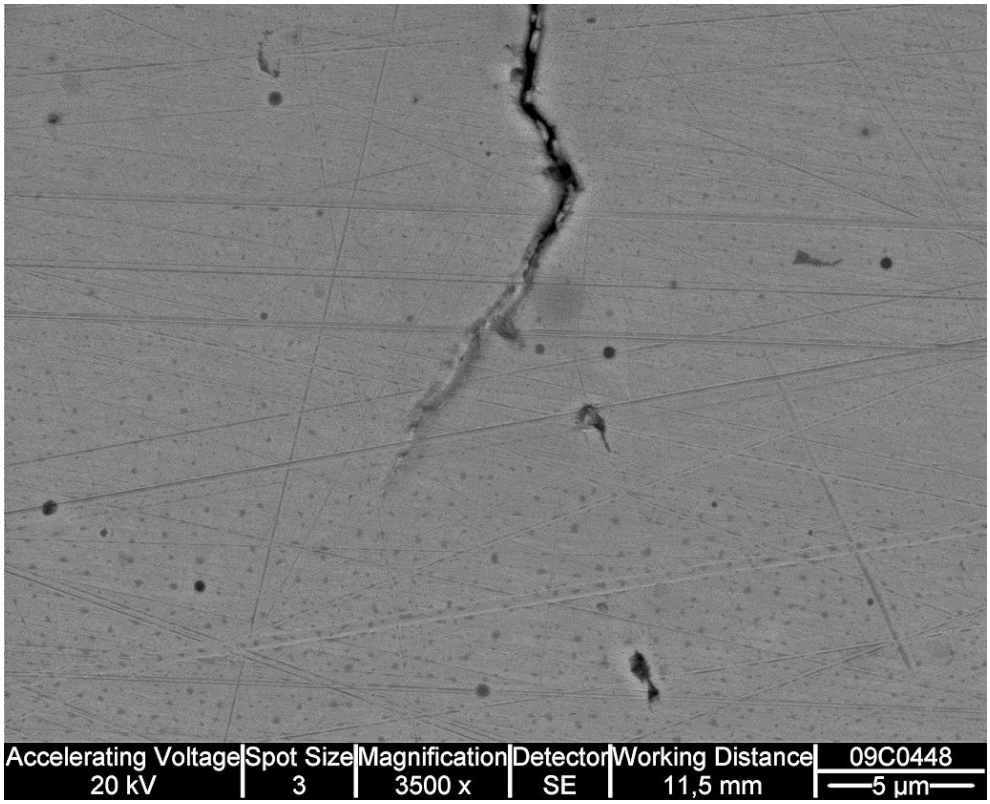

Figure 9: Viewed at higher magnification in SEM SE mode, it is evident that the cracks are filled with some compound, probably oxide, especially at the very tight crack tips.

TEM specimen slice TV4-7-4-1 was prepared from one of the deep, branched cracks of piece TV4-7-4, such that the primary crack tip and a side branch flank were both amenable to TEM examination, as shown in the images of Figure 10 and Figure 11. The appearance of those cracks in low-magnification TEM images at locations A, B and C are shown in Figure 12, Figure 13, and Figure 14, respectively. The crack in the first two images, hereafter referred to as "Crack A", appeared to be filled with a fairly uniform oxide all the way to its relatively blunt tip. The nature of that oxide is shown more clearly in Figure 15, which also shows what appear to be some globular particles within the crack at its narrowest point. Meanwhile, the side branch in location C was quite tight and irregular. In that location (tangential to the crack flank at that point), there also appears to be some globular phase at the foil edge.

For comparison, Figure 16 shows one of the shallow surface cracks, referred to henceforth as "Crack B." It has a rather wide mouth that quickly tapers to a narrow, oxide-filled crack. As shown in Figure 17, the oxide in this crack also tended to be fairly uniform in appearance.

Finally, Figure 18 shows a portion of the wake of one of the long, branched oxide-filled cracks, also from piece TV4-7-4, referred to hereafter as "Crack C." The oxide appears to be comprised of blocky particles adjacent to the base material, with the rest of the crack filled by a more uniform-looking phase. As shown at higher magnification in Figure 19, the oxide adjacent to the metal in Crack C is quite heterogeneous in geometry, with both light areas and dark areas, in both faceted shapes and more globular forms. Closer to the tip the crack would seem to be filled mostly with the larger, globular shaped oxide, as shown in Figure 20.

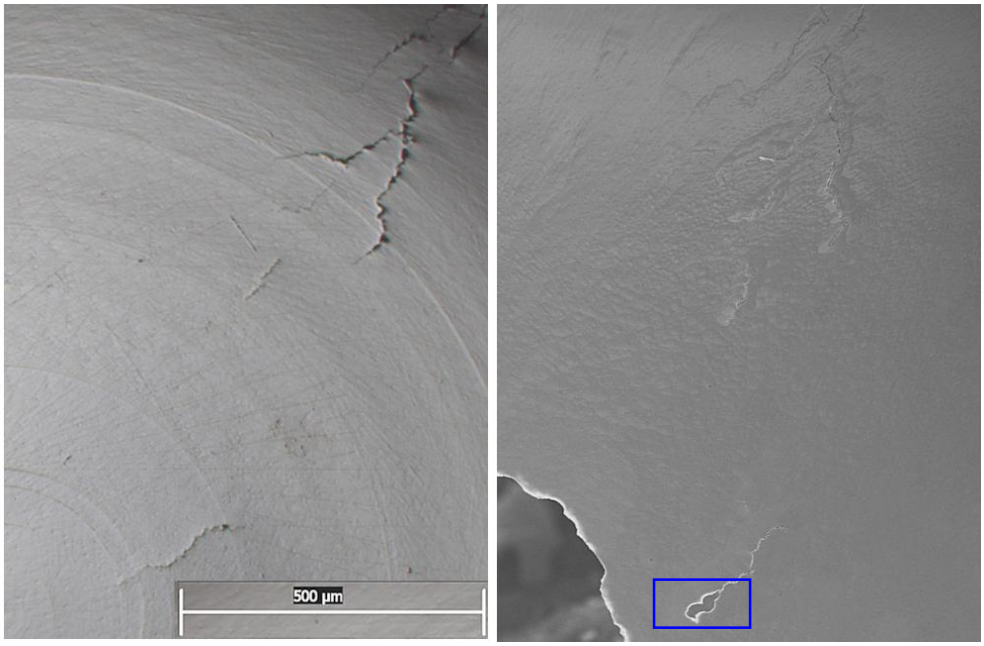

Figure 10: Specimen preparation of TV4-7-4-1, showing dimpled crack (left) and subsequent ion-milled crack (lower part of right-hand image).

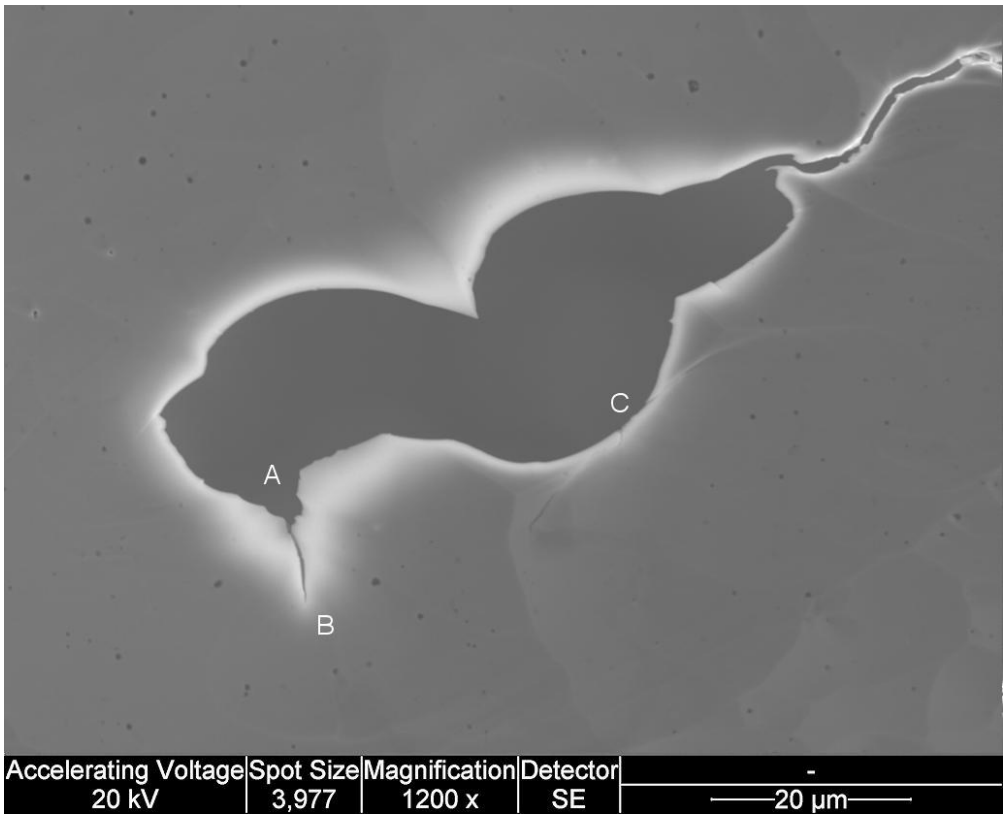

Figure 11: Closer SEM image of the electron transparent regions of the crack, from the area indicated by the blue rectangle in the previous image. The letters refer to the regions shown in the following images.

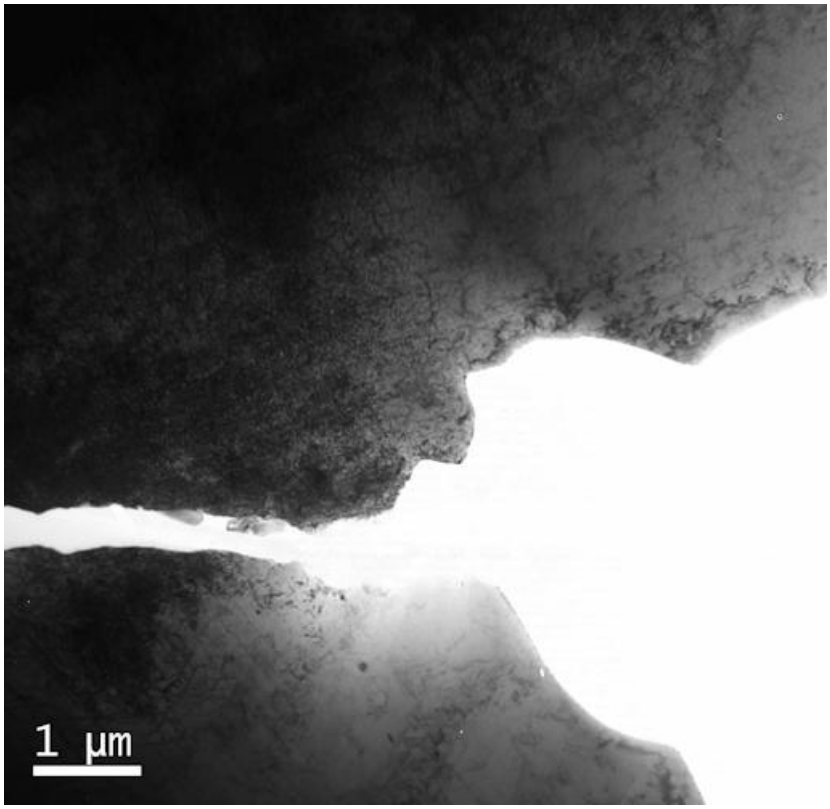

Figure 12: Region A of Figure 11, showing a portion of the trunk of "Crack A."

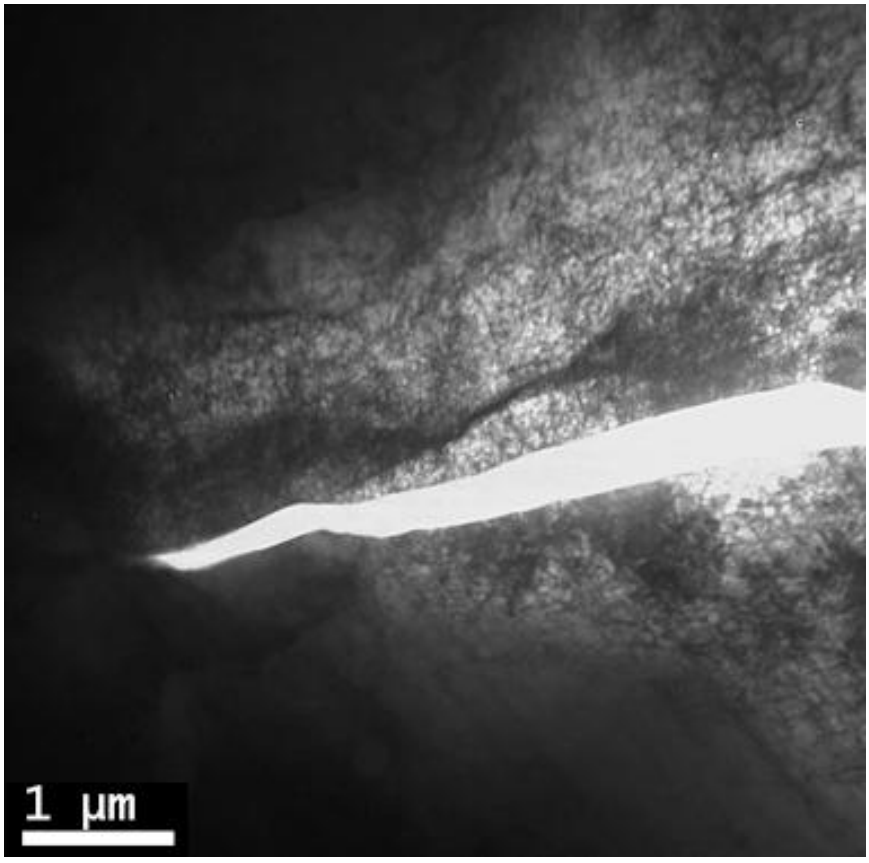

Figure 13: Region B of Figure 11, showing the apparent tip of "Crack A."

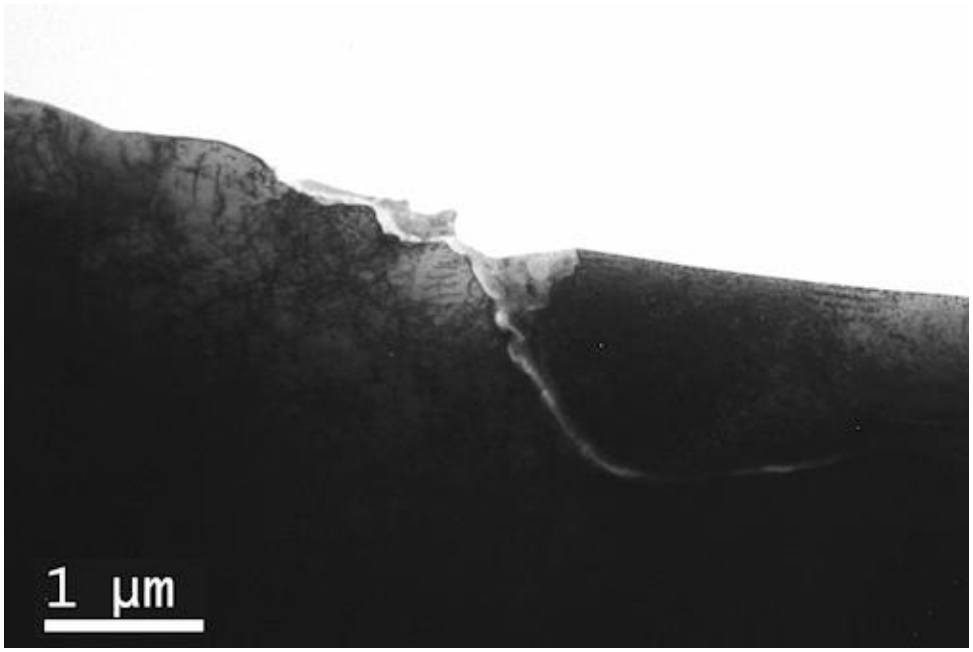

Figure 14: Region C of Figure 11, showing a side branch, probably of "Crack A."

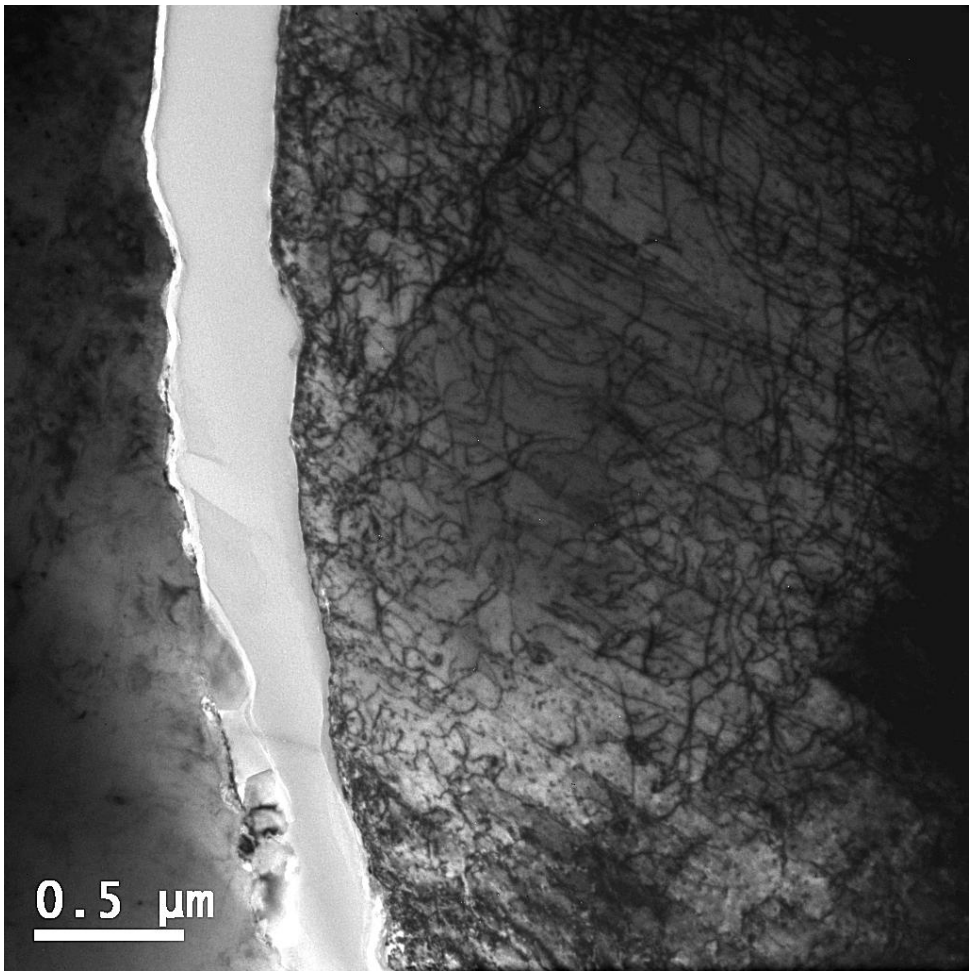

Figure 15: A closer examination of the oxide of "Crack A."

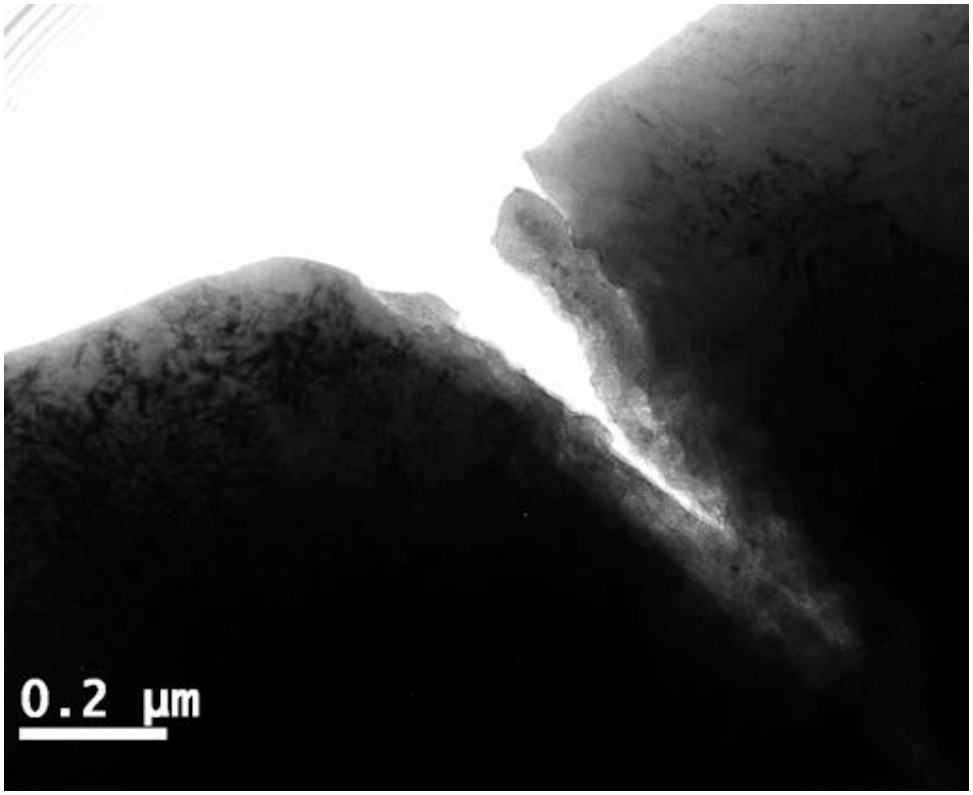

Figure 16: A shallow surface crack, "Crack B."

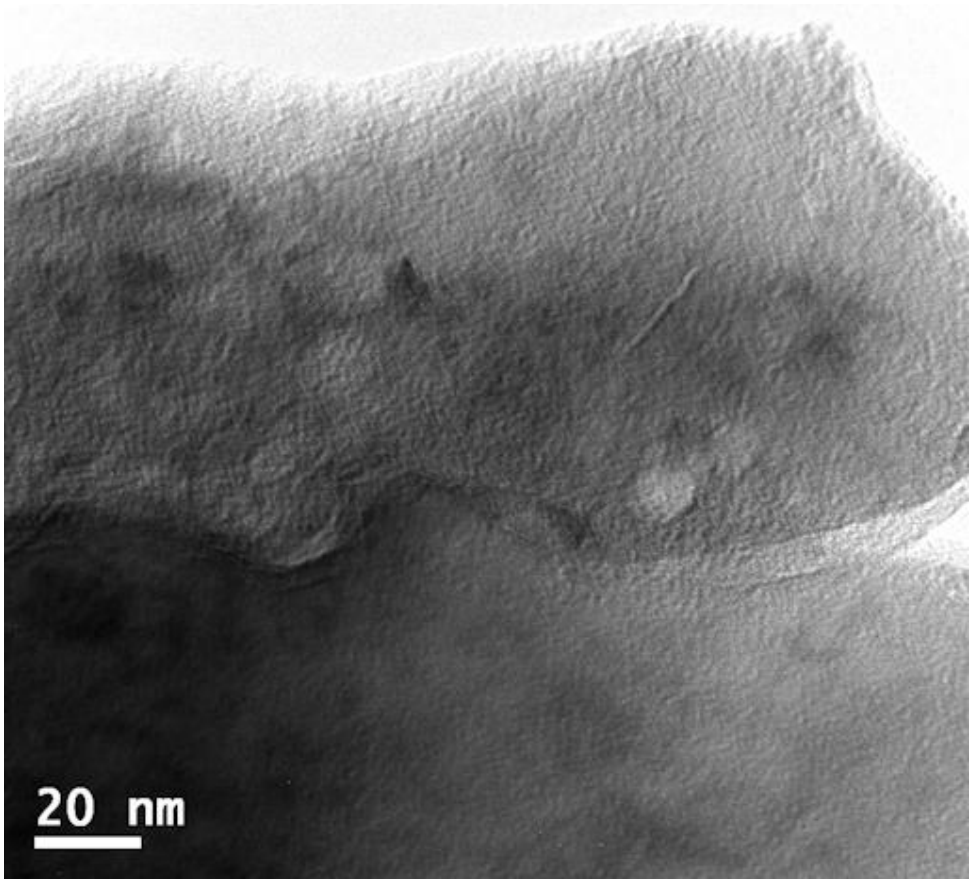

Figure 17: Closer examination of the oxide morphology in "Crack B."

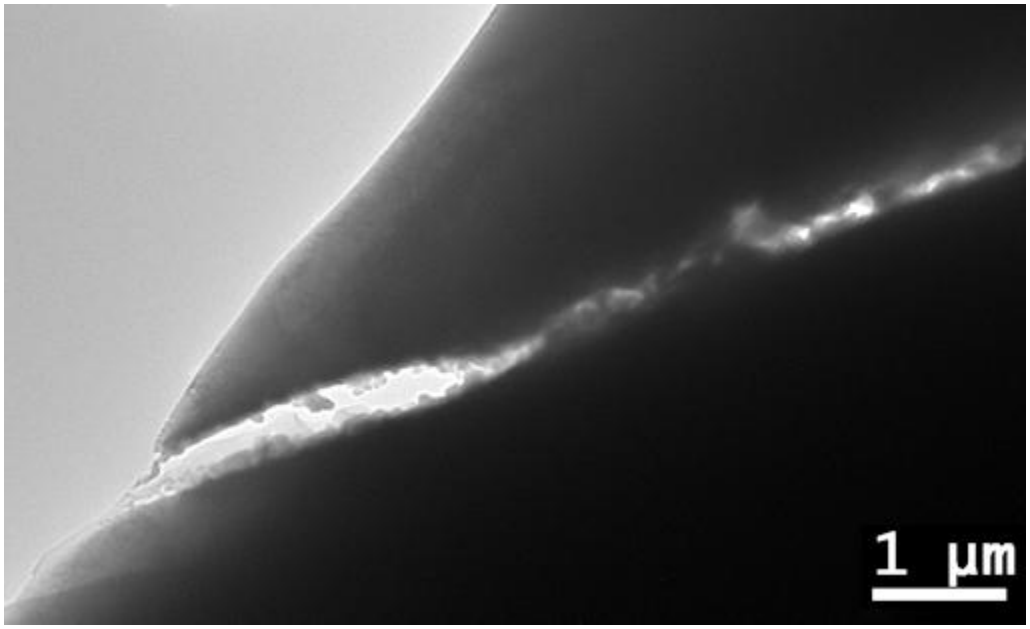

Figure 18: A portion of the trunk of one of the long, branched oxide-filled cracks from piece TV4-7-4, referred to as "Crack C."

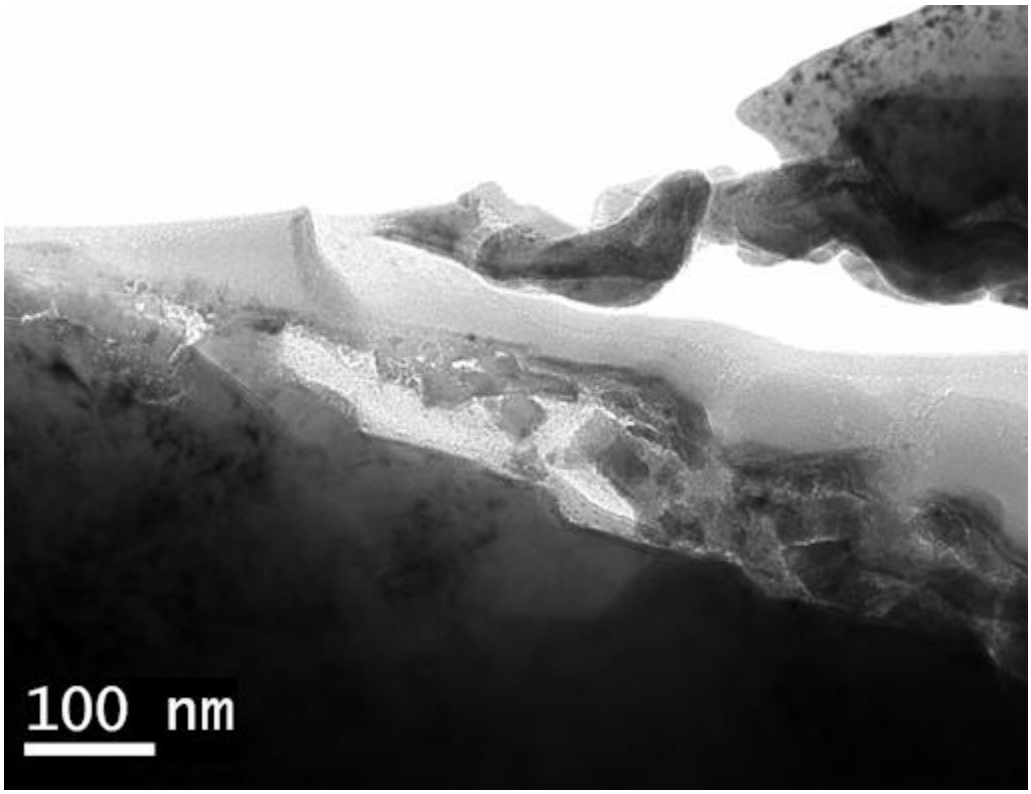

Figure 19: Crack C viewed at higher magnification. The oxide adjacent to the metal is quite heterogeneous in geometry, with both light areas and dark areas, in both faceted shapes and more globular forms. The middle region, meanwhile, is quite uniform and continuous in appearance.

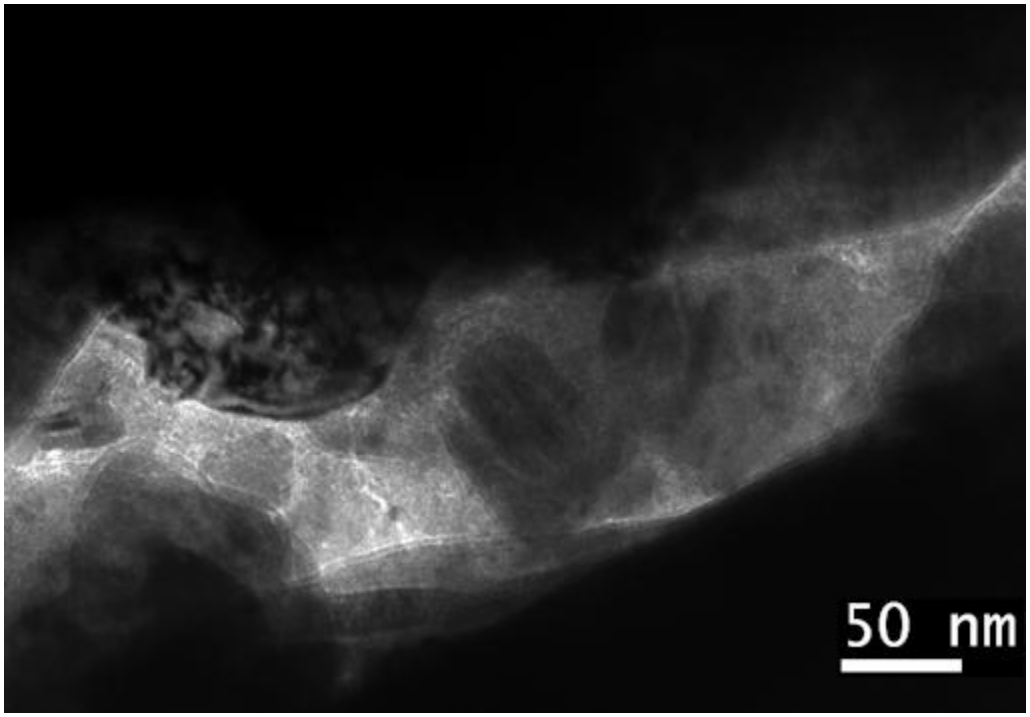

Figure 20: Closer to the tip, Crack C would seem to be filled mostly with larger, globular shaped oxide.

3.1 EDS Analyses

To better understand the nature of the oxides in these cracks, a number of EDS spot analyses were taken from different regions of the material filling the cracks. This is documented in more detail in the Appendix. In general, all of the crack examples had some features in common. In all regions of the oxides there was much less nickel than in the weld metal substrate, and likewise, generally more chromium. The oxygen content generally increased from the substrate towards the middle of the crack. The chromium content of the oxide structures was generally highest adjacent to the substrate, while in the substrate immediately adjacent to the oxide the alloy may have been depleted in chromium and iron. Dark, globular and angular particles were often found within the cracks, generally attached to one wall or the other. These were typically Nb-based particles rich in Mn (e.g. coated, co-segregated, etc. with Mn).

Each of the crack examples showed some key *differences* as well. Crack A showed the most uniformity in composition, generally showing the oxide region to be similar in composition to the weld metal, but having markedly lower nickel content and perhaps slightly higher chromium content than the weld metal. On an atomic weight basis, the oxygen increase was roughly commensurate with the nickel decrease and slight chromium increase. The particles, meanwhile, were mostly niobium with significant quantities of manganese. A similar uniformity in composition was evident in Crack B, with the exception that the oxide in Crack B *also* contained significant quantities of chlorine, some sulphur, and possibly fluorine (Appendix Table 11). Finally, the oxide in Crack C showed significant variability, particularly within the heterogeneous region close to the substrate. In that region there was significant spatial variation in the nickel, chromium, iron and

niobium contents. The darkest regions within this inner portion often showed significantly higher niobium and/or manganese contents, while substrate regions often showed depletion of iron and chromium. Meanwhile the lighter, more uniform region filling the middle of Crack C was particularly high in oxygen and tended to be much richer in nickel than in chromium or iron.

The compositional differences discovered within the different cracks' oxides prompted a more methodical analysis of them. That analysis data is shown in the Appendix (Tables A1-A6, A8-A10, A11). Figure 21 shows the compositional profiles at a wide region of Crack A. The figure illustrates the fact that the composition fluctuation is principally observed in the region adjacent the crack wall, and that the primary actors would seem to be Ni and O atoms. The Ni and O ratio is roughly 1:1. The other principle elements also appear to be present, at about the same level as in the weld material. This would suggest an oxide having metallic atoms in the ratio 2Ni:1Cr:1Fe, with some incorporation of Mn and Si as well. Another profile of Crack A, across the whole crack and at closer measurement spacing, is shown in Figure 22. It shows a similar trend as the previous profile for the metallic atoms in the middle region, but with a higher oxygen content indicated. On the other hand, immediately adjacent the crack walls on each side there appears to be some fluctuation in the composition, with a depletion and then enrichment of Ni, Cr and Fe, and an opposite trend of enrichment and depletion of O. On the right hand side there is also an apparent peak in Si and dip in Mn, while on the left hand side there is a dip in the Si content. The O content appears to reach a maximum at the middle of the crack.

For comparison, Figure 23 shows profiles measured from Crack B, particularly focused on the region adjacent the crack wall. Crack B also exhibited a fluctuation in Cr near the crack wall, with its peak occurring in a region about 20-30 nm wide close to the substrate. As in the case of Crack A, the Ni content seemed to mainly reflect the inverse of the O trend, with the exception of the higher Cr region. Particularly interesting in the profiles of Crack B, however, is the presence of Cl. The Cl content was remarkably high, particularly on either side of the higher Cr region. The presence of Cl was evident only in Crack B, and was not found in Crack A nor Crack C.

The oxide structure in Crack C was much more heterogeneous than in Crack A and Crack B. Nonetheless, some example trends for each element as a function of distance from the apparent metal/oxide interface are shown in Figure 24, collated from miscellaneous exploratory spot analyses. Since the interface was not distinct nor uniform, the precision of the collection locations was only about ±10 nm. Despite the heterogeneity, the composition appears to fluctuate in a manner similar to that of Crack A and Crack B, clearly displaying the Cr-rich region at the crack wall. However, Crack C exhibited much more Cr enrichment than Crack A or Crack B, while its O profile no longer followed the inverse of the Ni content so closely in the oxide region. Also apparent from the trends is the similarity in behaviour between Fe, Cr and Mn, while the Ni fluctuated more independently.

Thus, while in each of the example cracks the magnitude of composition fluctuated somewhat differently, in all cases there was a chromium-rich inner region at the crack wall and a more nickel-rich outer region.

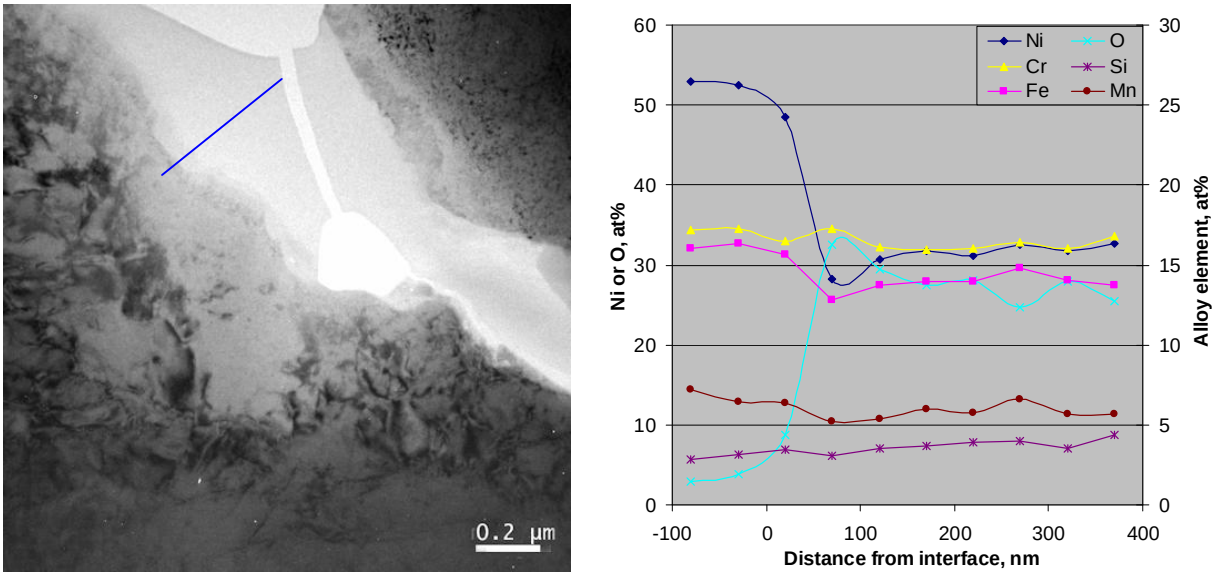

Figure 21: Composition profile in atom percent for a wide portion of Crack A, along the blue line shown in the image.

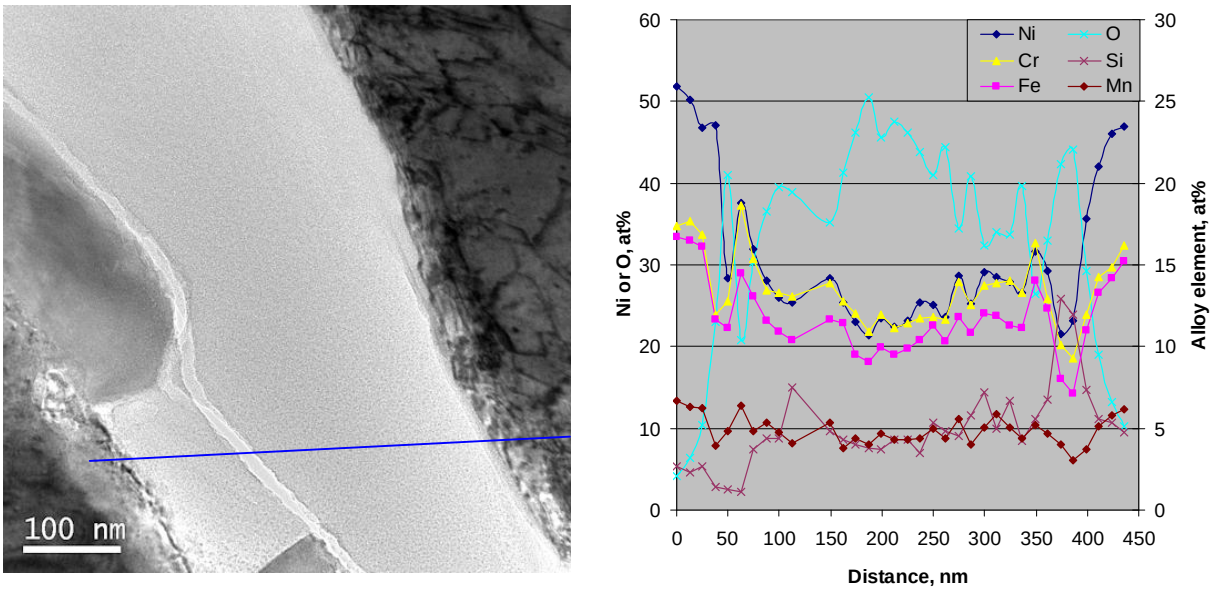

Figure 22: Composition profile in atom percent for a narrower portion of Crack A, along the blue line shown in the image. The large grey particles visible on the left and bottom of the image are niobium and manganese rich.

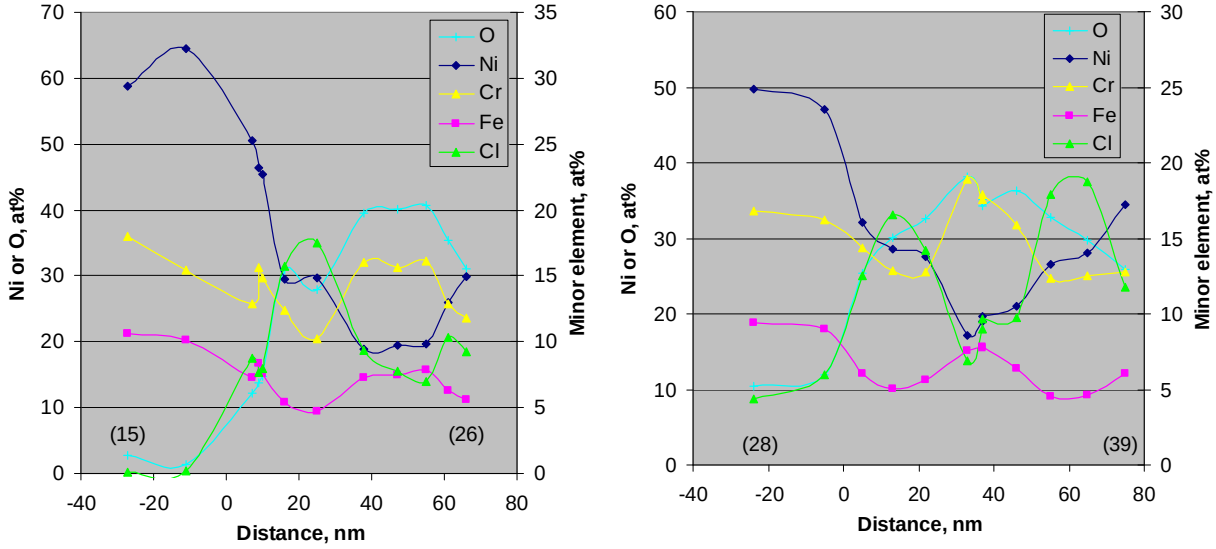

Figure 23: Composition profiles in atom percent for two different portions of the Crack B oxide, focused on the region closest to the substrate (i.e. crack wall). There is a chromium-rich inner layer occurring in a region about 20-30 nm wide. Of particular interest is the presence of chlorine, particular located on either side of the Cr-rich region. Fluorine and sulphur were also detected in Crack B oxide, though at lower amounts than the Cl.

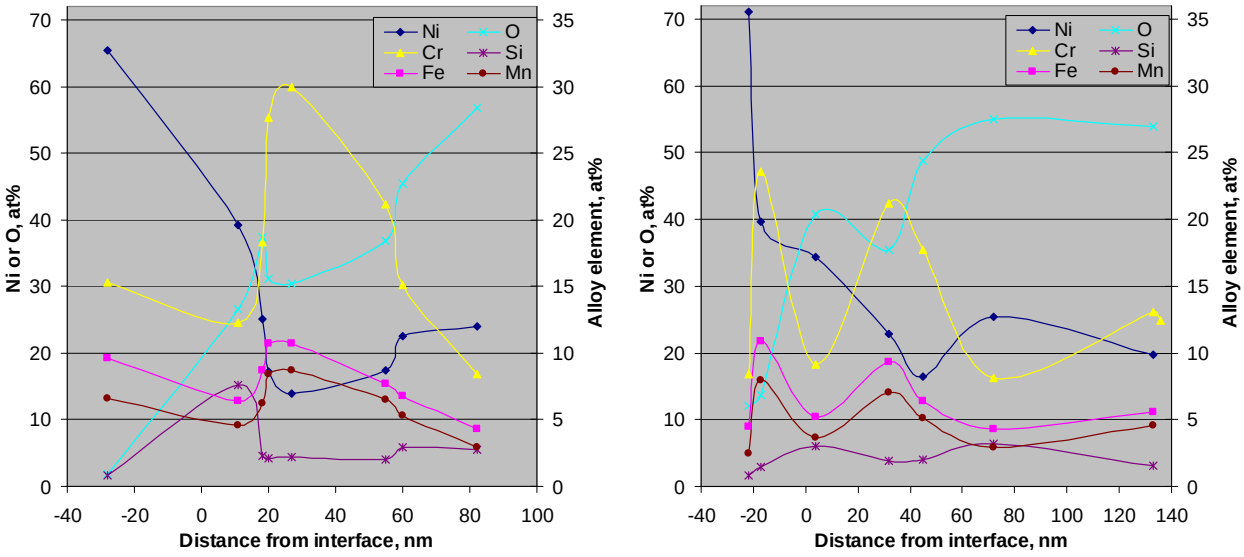

Figure 24: Composition profiles in atom percent for the oxide of Crack C, compiled from miscellaneous spot analyses. The figures clearly show a Cr-rich region a few tens of nm wide at the crack wall, in this case showing much more Cr enrichment as compared to that in Crack A or Crack B. In these cases the O profile no longer follows the inverse of the Ni content so closely in the oxide region though.

3.2 SAD of crack oxide structure

Electron diffraction was utilized to try to better understand the structure of the oxides. The SAD effort is described in more detail in the Appendix (Figures A49-A52, A62-A69 and Figures A97-A99.) In general though, it was found that even the smallest selected area aperture was still too large to permit any clear structural differentiation between the Cr-rich inner portion of the oxide and the outer oxide filling the cracks. Instead the SAD patterns were often populated by a conglomeration of what were probably a number of different diffraction patterns for different grains and structure types simultaneously, preventing unambiguous identification of individual regions.

Nonetheless, Figure 25 shows one of the best SAD pattern examples found, which was recorded from the more uniform oxide in the middle of Crack C. The ring-type SAD pattern containing discrete spots indicates that the structure is nanocrystalline, with randomly oriented grains simultaneously diffracting. As demonstrated in the Appendix, the distribution of the rings as a particular series of pairs and singular rings of specific diameters suggests that the structure is face-centered cubic (FCC). Calculations based on the measured diameters of those rings indicated that the oxide had a lattice parameter of a_o = 3.905 Å. For comparison, a NiO type of oxide also has a FCC structure, but its lattice parameter in pure form is a_o = 4.179 Å. That would produce a SAD ring pattern having the same ring periodicity, but of slightly smaller diameter.

On the other hand, the EDS analyses consistently indicated the presence of Cr and Fe (and often Mn as well). Such mixed-composition oxides often take on the form of a diamond-cubic structured spinel oxide, having a version of the stoichiometery AB_2O_4, where A is a divalent Ni (or Fe) ion and B is a trivalent Cr or Fe ion [2]. In its pure form, a chromium oxide spinel has a lattice parameter of a_o = 8.36 Å, and would exhibit diamond-cubic ring periodicity in SAD. When such a ring pattern was superimposed on a diffraction pattern composed mostly from the more heterogeneous inner layer of the oxide of Crack C, a reasonable fit was achieved, as shown in Figure 26. It may be that the model ring pattern is slightly smaller than that of the actual ring pattern of the image, which would suggest a slightly smaller lattice parameter in the actual oxide. However, the poor quality of the diffraction pattern prevented such a calculation from being satisfactorily achieved. The fact that some of the spots along the rings are much brighter than others indicates some preferential orientation in some particular directions, possibly in relation to the substrate metal.

The oxide of Crack B was also examined with SAD. Though the result was much less clear, it seemed that the spinel oxide ring pattern was a better fit than that of an idealized NiO or of the FCC oxide identified in Figure 25.

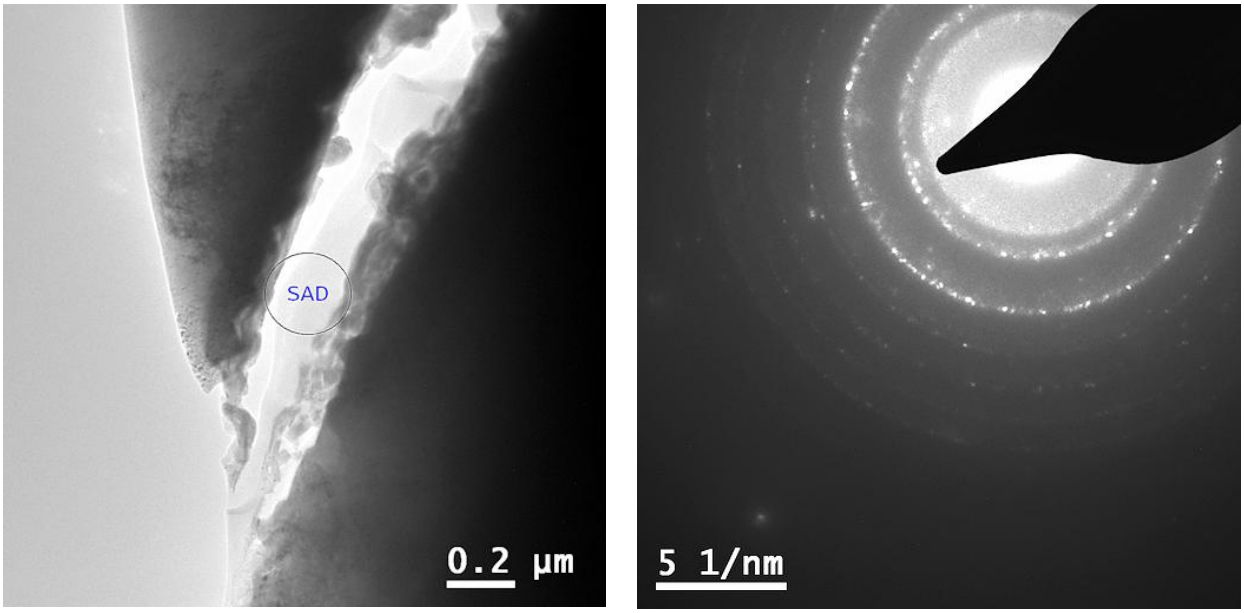

Figure 25: An example of a SAD ring pattern from the more homogeneous oxide in the middle Crack C (location indicated in left hand image) suggested a face-centered cubic (FCC) structure having a lattice parameter a_o = 3.905 Å.

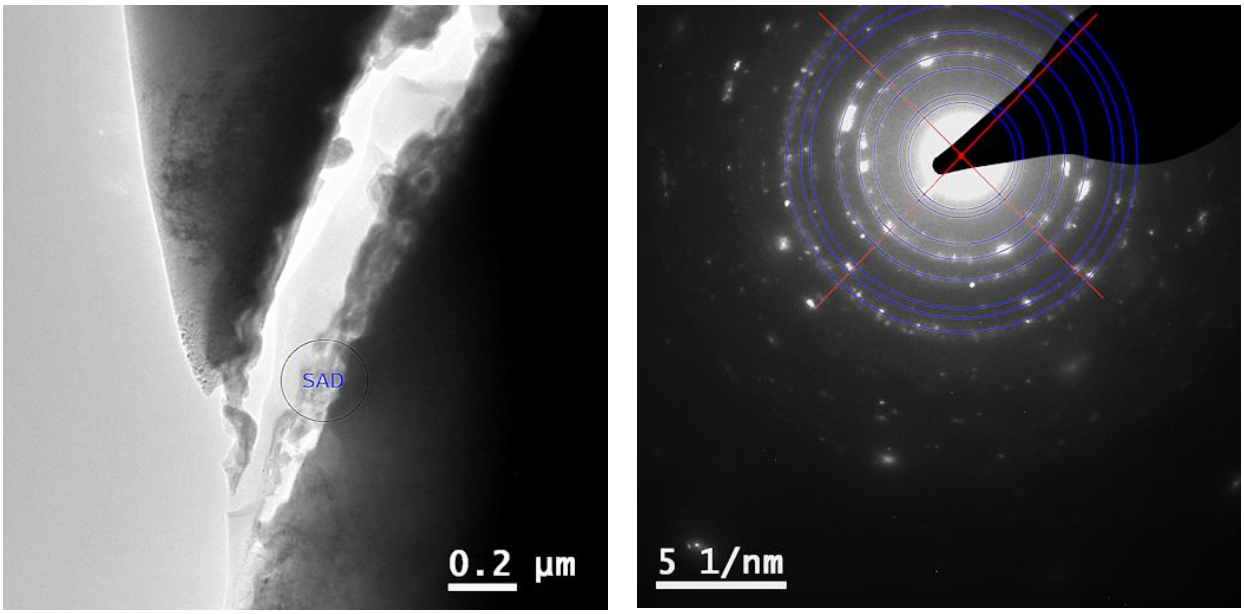

Figure 26: An example of a SAD ring pattern from the heterogeneous oxide at the crack wall of Crack C (location indicated in left hand image) suggested a diamond cubic structure similar to the idealized version of a spinel oxide having a_o = 8.36 Å (overlay rings in right hand image).

Crack A offered an opportunity to examine the relationship between the oxide and the matrix, as shown in the series of images in Figure 27. As demonstrated by the solutions shown in the Appendix (Figures A29-A37), the SAD patterns indicate an epitaxial NiO formed in a distinct orientation relationship with the matrix. While SAD32 is comprised principally of the Ni alloy matrix spots with only a minor presence of a ring of NiO spots, SAD30 mostly indicates an almost amorphous NiO, with the pair of bright spots from the Ni alloy matrix only

faintly visible. However, SAD31 shows more predominate NiO rings, with greater crystallinity indicated by the rings of equally spaced, but separate spots. The Ni alloy matrix spots are much more evident in SAD31 as well, and the orientation relationship between the two phases is apparent as the inner ring of spots enclosed by a square of matrix spots (a pair of primary spots and a pair of spots resulting from double diffraction with the oxide). Noteworthy is that the lattice parameter in this case is closer to that expected for pure NiO. The amorphous character in the outer oxide may be an artefact of the ion-milling, which is known to produce a thin amorphous layer, which would then be more apparent in extremely thin regions like that of SAD30.

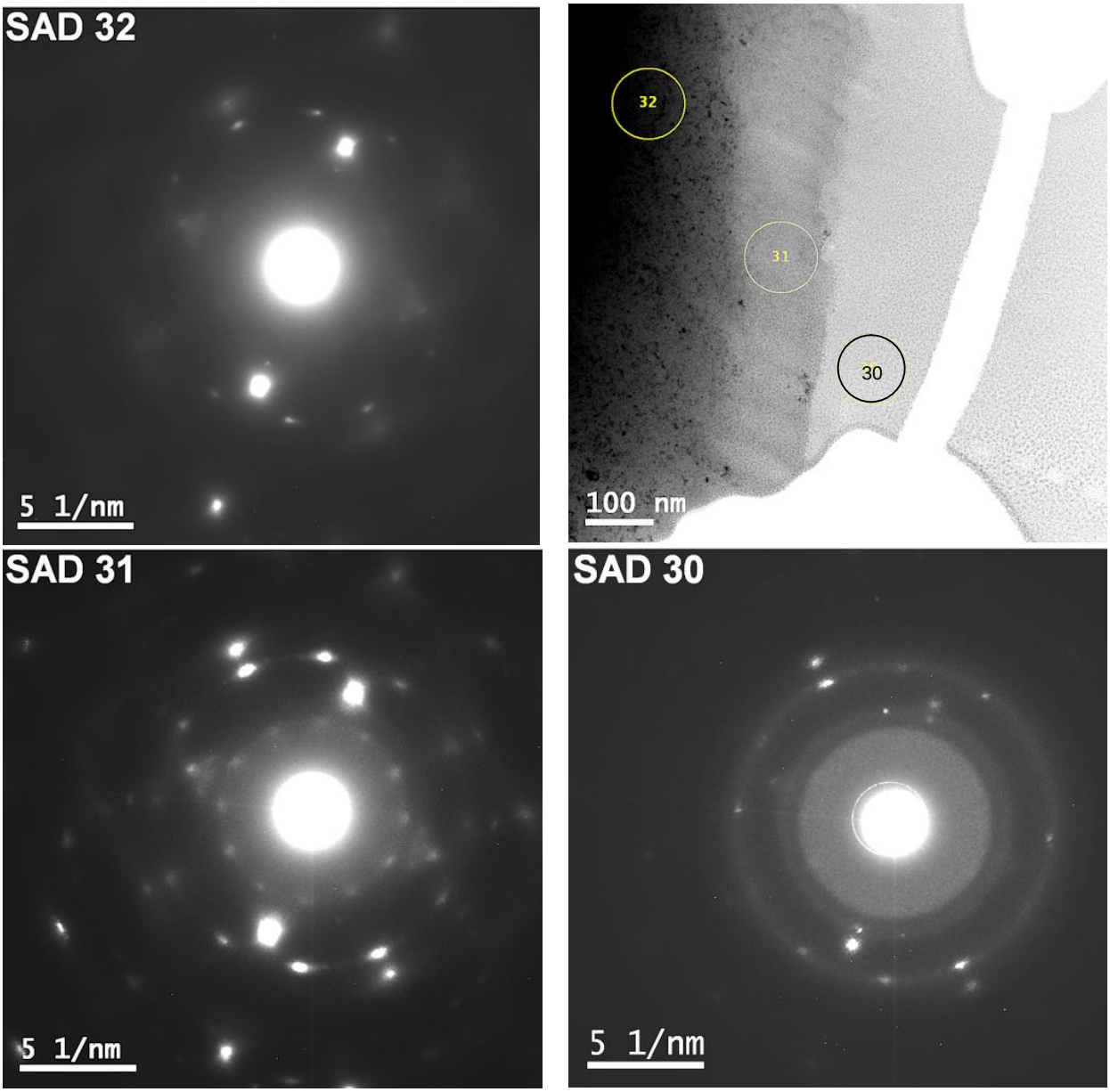

Figure 27: SAD patterns of three oxide/matrix regions in Crack A, showing an apparent epitaxial oxide formation. SAD30 mostly indicates an almost amorphous NiO, with a couple of bright spots from the Ni alloy matrix. SAD31 shows much more predominant NiO with greater crystallinity indicated by the rings of equally spaced, but separate spots. The Ni alloy matrix spots are much more evident as well, and the two phases share an orientation relationship. Finally, SAD32 is comprised principally of the dominant pair of Ni alloy matrix spots, with only a minor presence of the larger ring of oxide spots, and no inner ring of spots.

4 Discussion

The EDS and SAD results for the three different crack examples suggest that two kinds of oxides may be present, and that they seem to be arranged as an inner layer immediately adjacent to the crack wall and an outer layer filling the rest of the crack. The SAD analyses indicated that the oxides may take on either a diamond-cubic spinel structure or a face-centered cubic NiO type structure, in some cases having a slightly smaller lattice parameter than the pure counterpart. The EDS analyses indicate that the inner layer is richer in Cr and Fe than the outer layer, but the oxide is still predominately Ni rich.

4.1 Crack and oxide character

As was described earlier, mixed-composition oxides often take on the form of a diamond-cubic spinel oxide having the stoichiometery AB_2O_4, where A is a divalent Ni (or Fe) ion and B is a trivalent Cr or Fe ion [2]. Thus, in its purest form the combined Cr and Fe content of such a spinel should be at least double its Ni content. Figure 28 shows the Cr+Fe amount plotted with the Ni and O compositions for the oxides of each crack. Immediately evident from those plots is that in Crack B and Crack C the Fe+Cr content exceeded the Ni content in the region of the Cr-rich inner oxide. In particular, in Crack C the 2:1 ratio of (Cr+Fe):Ni was clearly fulfilled in the inner layer, the same region from which the spinel SAD pattern was recorded (Figure 26). Thus, the inner oxide of the cracks is most likely comprised mostly of a Cr (Fe)-rich spinel.

By contrast, in the outer oxide layer of Crack C a clear NiO type SAD pattern had been recorded (Figure 25), corresponding to the region where the Cr and Fe contents were back to about the same levels as they had been in the substrate adjacent to the spinel layer. Similar SAD findings were made for the Crack A oxide, which was shown to have an epitaxial NiO structure (Figure 27) while the Cr and Fe tended to fluctuate synchronous with the Ni content, at about a (1+1):2 ratio (e.g. Cr+Fe = Ni). Although the quantification of the exact oxygen content via EDS is unreliable, the stoichiometry at the middle of Crack A reached about Ni_2CrFeO_4. Therefore it is plausible that the oxide in Crack A is primarily NiO, with the other elements (Cr and Fe, and possibly Mn and Si) simply being incorporated into the lattice in approximately the same amount as they were present in the matrix, in the place of Ni ions. While some Cr fluctuation was observable at the crack walls, in that particular specimen the examined area was close to the actual crack tip, so the situation may represent an active crack.

Meanwhile, Crack C would then seem to represent a mature/stagnant stage of crack, in which the initial Cr- and Fe-containing NiO has decomposed into a more obvious two-layer oxide comprised of an inner layer of Cr (Fe)-rich spinel oxide and an outer layer of NiO. Leaching of Cr and Fe from the substrate (crack walls) could expand the crack width while redistribution of Ni could then be occurring at the outer oxide, filling the crack. This is plausible also from the perspective that the examined portion of Crack C was some distance behind the crack tip, in the wake of the crack. Therefore, Crack C could represent an evolved form of Crack A.

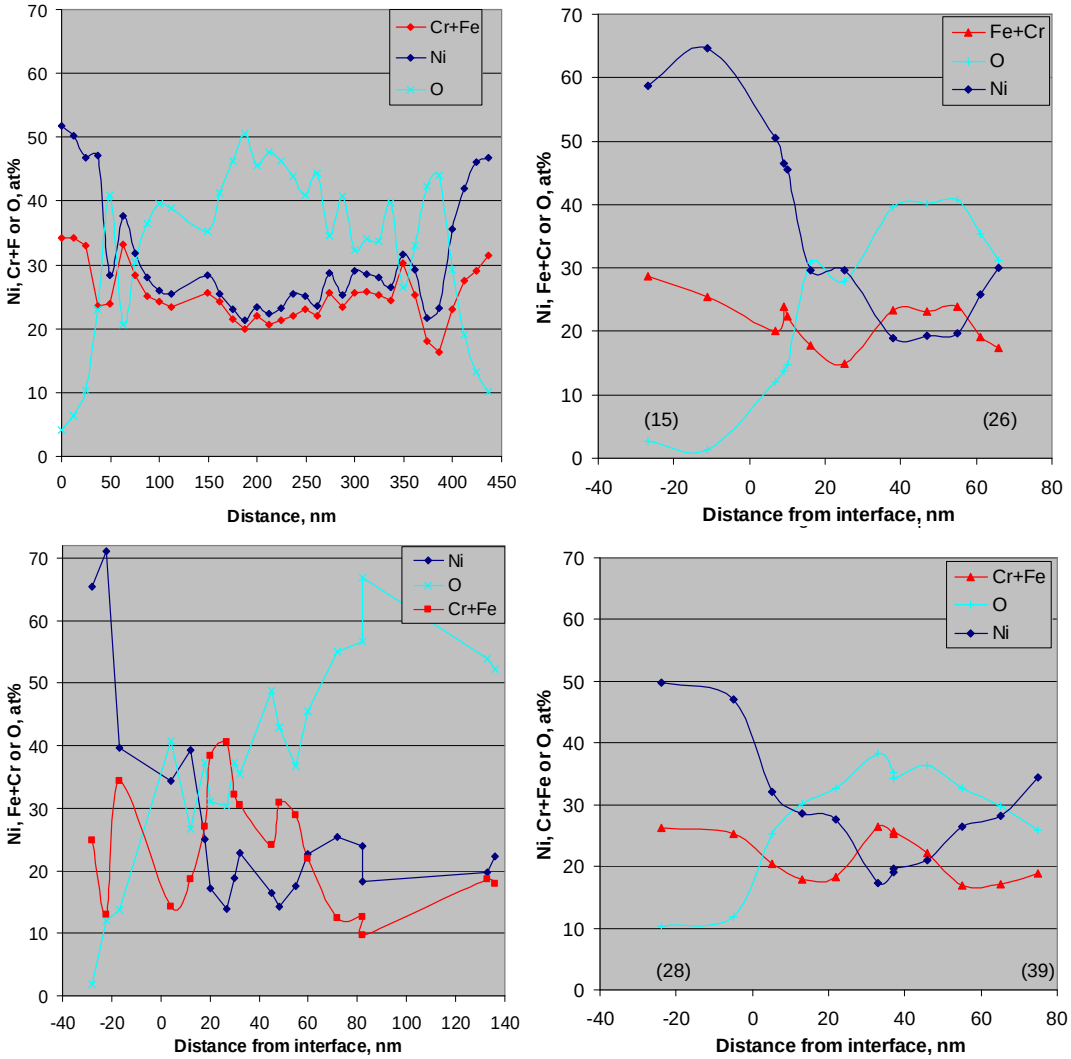

Figure 28: Plots of the combined Cr and Fe content in comparison to the Ni and O profiles for oxides in (clockwise from upper left) Crack A, Crack B, Crack B and Crack C.

Such a decomposition process could be represented by Crack B, which would seem to be in a transitory stage. While the SAD of the Crack B oxide suggested that a spinel-type oxide was present, some spot formations may have been more attributable to a NiO, and overall they were difficult to separate confidently (Appendix, Figures A98 and A99). Likewise, the Cr+Fe amount only exceeded the Ni content at the peak of the inner oxide layer, and even there the ratio did not yet approach 2:1. The extent of segregation in Crack B versus Crack C is illustrated in Figure 29, where individual element profiles are collated (in weight percent) for point analyses of the oxides of Crack C (solid symbols) and Crack B (open symbols). In both cases the tendency for Fe, Cr and Mn to coexist in the inner oxide is apparent, but in Crack C the variation in composition is even greater. Thus, Crack C would seem to be a more evolved stage of Crack B.

Also noteworthy with respect to Crack B was the presence of Cl and possibly S and F, which were not found in any significant amount in the other cracks. The super-critical steam was intentionally doped with impurities of chloride, sulphide and fluoride to enhance crack initiation. The discovery of those impurities in Crack B, coupled with the fact that Crack B was a very shallow crack like that

shown in Figure 7, indicates that Crack B most likely represents a crack that initiated, but did not grow very far before it arrested. The formation of the Cr-rich spinel inner layer then proceeded. The formation of a NiO prior to the Cr-rich spinel is supported in this case also by the observation that the Cl was associated more with the NiO than with the Cr-rich spinel.

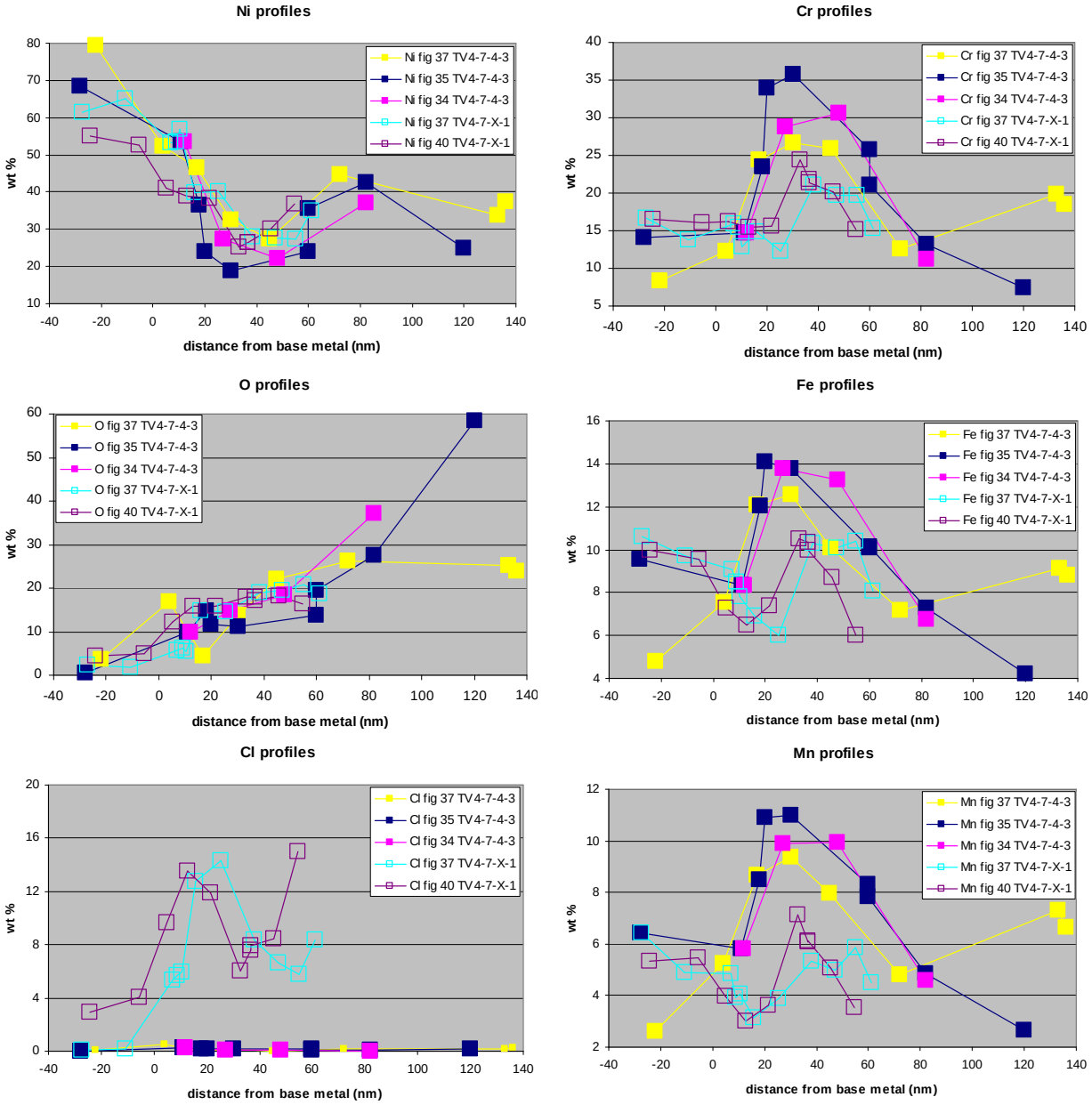

Figure 29: Collated element profiles in weight percent for point analyses of the oxides of Crack C (solid symbols) and Crack B (open symbols). In both cases the tendency for Fe, Cr and Mn to coexist in the inner oxide is apparent, but in Crack C the composition variation was even greater. The presence of Cl is evident only in Crack B, and was not detected in Crack A or Crack C.

4.2 Comparison to literature

The true conditions within a crack in doped steam are not known. However, while the literature on nickel alloy oxides is mostly focused on tests carried out on specimens immersed in hot water, some parallels may be possible between that and the doped steam environment. The literature for tests in hot water supports the possibility of both a NiO and a Cr-rich spinel oxide coexisting in nickel-based alloys. As summarized in the literature review VTT Research Report BTUO73-041285 [3], bi-layer oxide film structures are typically observed in nickel-based alloys, but the film formation kinetics are generally considerably slower than that on stainless steels, even at a high oxidative power of the environment, producing thinner films with smaller crystallite size than for stainless steels in comparable conditions. The report further describes that Cr enrichment in the films has been observed especially in the inner layers formed in PWR primary and secondary side coolants. It adds that the films on nickel-based alloys do not exhibit spinel structures alone, but depending on the extent of reducing power of the environment (e.g. the concentration of dissolved hydrogen in the PWR water), they also contain either NiO or elemental Ni. According to that literature review, at short exposure times in PWR conditions the films contain essentially Cr_2O_3, whereas $Ni(OH)_2$ and NiO are formed for longer exposure times or in the presence of higher content of NaOH. The effect of temperature on the surface film composition in lithiated water is such that substantial Cr enrichment is observed in the temperature range 250-300 °C only, with nickel being the main cationic constituent of the films for temperatures below 250 and above 300 °C. Finally, the literature review pointed out that long-term exposure in PWR water generally produces inner layers of spinel+NiO(or Ni) and outer layers enriched in Fe, stating that it has been demonstrated that perhaps due to the immiscibility of the spinel phases such as $NiCr_2O_4$ and $NiFe_2O_4$, the outer layer on nickel alloys after prolonged exposure can act as a sink for Fe from the coolant.

The oxides found in the cracks of this study, produced by four-point-bend testing in doped steam, reflected similar features as described for the nickel alloys exposed to PWR water conditions, but there were still some key differences. Firstly, while Fe was present in both the inner and outer layers of the crack oxides of this study, it did not appear to be particularly enriched in the outer layer, rather tending to be enriched in a manner similar to Cr. That is probably because, in doped steam, the possibility for liquid coolant exchange does not exist, so the oxide is not serving as a sink for Fe from the coolant, as described for immersion tests in PWR conditions. Also, although Cr enrichment was clearly present in the inner oxide layer, it could not be described as substantial in most cases, and the width of that inner layer (~30-50 nm) tended to be only a small portion of the overall width of the oxide-filled crack.

Alternatively, Lozano-Perez and Titchmarsh [4] carried out analytical TEM of SCC cracks initiated in Inconel 600 following constant load tests in PWR primary water conditions, and found that cracks seemed to initiate and grow at chromia formed at grain boundaries intersecting free surfaces and blunted, open cracks, but found that open cracks were filled with nano-crystalline NiO and large compound particles of spinel and NiO. They attributed that distribution to a difference in potential between closed, attacked boundaries and open cracks. That would suggest that the findings of the current study may principally represent the latter scenario,

whereas closer examination of surface regions could reveal the internal oxidation of grain/dendrite boundaries that precede crack opening.

On the other hand, the description by Thomas et al. [4] for the oxides in SCC cracks of nickel-based alloys suggests that an epitaxial based on the NiO can be the first oxide to form, due to the lack of sufficient Cr to promote the Cr-based spinel expected by thermodynamics . Such behaviour would seem to be the more likely case for these materials tested in doped steam, since Crack A showed an epitaxial relation between the NiO and the substrate, and in the other cracks the spinel oxide layer in general still contained significant quantities of Ni as well. This is supported by the earlier statement that in lithiated water Ni enrichment is preferred over Cr enrichments at temperatures above 300°C (the doped steam test was carried out at 400°C).

Likewise, in conducting analytical TEM of primary-side cracks in an Alloy 600 nozzle head penetration and its accompanying Alloy 182 J-weld of the David Besse PWR, Thomas et al. [6] described a “complex IG corrosion behaviour” in which oxidation progressed along the dendrite boundary, reacting the carbides and other segregation found there, producing corrosion products containing Nb as well as Mn and other minor alloying elements in addition to the principal alloy elements. Similar oxidation of all the interdendritic species occurring in the doped steam cracks of this study would explaining the complex diffraction patterns and heterogeneity in composition observed within the cracks (including the presence of Nb and Mn), particularly evident in Crack C.

On the other hand, following the doped steam tests the compositions of similar cracks were also mapped by FEG-SEM EDS, and those findings seemed to indicate that many such cracks were filled with metallic nickel, particularly large cracks (~4 micron), especially at the open crack mouths. However, the cracks of this TEM study were examined close to their tips where the width was < 1 micron, and they did not seem to exhibit any metallic Ni filling the cracks. This would indicate that perhaps the existence of pure nickel represents a final stage of evolution of the cracks, following the growth of the chromium-rich spinel. It may be noteworthy that in NiO the M:O ration is 1:1, whereas in the spinel it is 3:4, so if there is only a limited amount of oxygen available in the doped-steam tests, then perhaps at the outer oxide regions there would be a return to metallic Ni as the oxygen diffuses inward to react with the growing Cr-rich spinel. Such a scenario would require reducing conditions in the crack though, and the exact conditions existing in the crack during the doped steam test are not known. Nonetheless, H. Hänninen et al. [7] recently theorized that such reducing conditions are possible because of the relationship between the Ni stability and the local hydrogen content in the crack. As he states, the Ni stability region is close to the H_2 –H_2O line in high temperature water, while the stability regions of Fe and Cr are below the line. Further, the critical H_2 fugacity varies with temperature, and increasing the H_2 fugacity causes the corrosion potential to decrease into the Ni stability region. Since the hydrolysis reaction of metal ions (Cr, Fe, etc.) produces additional H^+ /H_2, inside the cracks, the increased H_2 fugacity lowers the Ni^{2+} and NiO stability, enabling metallic Ni to be deposited. Therefore, it could be that metallic nickel would be found only once the Cr-rich spinel had substantially grown.

Finally, of particular interest to power plant operation is the potential relationship between hot-cracking and EAC crack initiation and/or propagation. In fact, as shown in Figure 5 and Figure 6, some cracks were found in the cross-sections which exhibited tearing type behaviour, but they did not seem to contain any oxide. Analytical TEM investigations were carried out earlier in the PERDI project on the same Inconel 182 weld material, but in the as hot-cracked condition. The findings indicated that the hot cracking was typically associated with the significant segregation of minor and trace alloy elements as a eutectic at the weld dendrite boundaries, which then tended to tear as a consequence of significant residual strains arising from the mismatch between the matrix and eutectic [8]. Such cracks were generally rather wide, with a sharply jagged path and smooth, undulating fracture surfaces, and ended in a rather blunt tip. In the current study the EAC cracks were very heavily branched and quite narrow and sharp towards their tips. While Nb- and Mn-rich regions were indeed found within the oxides, the composition overall was not as consistently heterogeneous as had been observed in the eutectic regions in advance of hot cracks. Likewise, Crack B in this study was clearly initiated at the surface, immediately taking on similar characteristics as the other cracks, whereas hot-cracks have been shown to occur within the material itself, without necessarily intersecting the material surface. Similar observations of EAC occurring independent of hot-cracking in Alloy 182 were made by Thomas et al. in their examinations of Alloy 182 safe-end nozzle weldments from Ringhals-4 PWR [9] as well as the aforementioned primary-side cracks in an Alloy 600 nozzle head penetration and its accompanying Alloy 182 J-weld of the David Besse PWR [6].

5 Summary and Conclusions

This study examined the oxide compositions and structures found in cracks produced in a four-point bend test bar that was exposed to an environment of steam doped with Cl, F and S ions at 400°C. Three different example cracks were extracted from the test bar, two from near the tips of deep cracks (Cracks A and C), and one shallow, surface crack (Crack B). EDS and SAD results indicated that two main kinds of oxides were present, containing mostly nickel, but arranged as a 30-50 nm wide Cr- and Fe-rich inner layer showing spinel structure, and an outer layer having NiO type structure filling the rest of the crack. A significant amount of Cl as well as some F and S were detected in the oxide of the surface crack. Based on the observation of an epitaxial relation between the NiO and the matrix, as well as the relative thicknesses and composition variations in the different oxide layers, it would seem that the dopants served to initiate the crack, and then once initiated, the formation of the NiO was dominant. The Cr-rich spinel inner layer then subsequently grew at the interface with the matrix, becoming thicker and more Cr- and Fe-rich as it evolved, perhaps promoting the transport of Ni metal ions towards the outer oxide surface. Such behaviour is counter to that typically expected for PWR environments, but at this moment the real conditions existing in the crack during doped steam testing are unknown, so the drivers of the crack oxide evolution in doped steam are not self-evident. This summary report is focused on the results analysis and discussion.

References

1. VTT Research Notes 2399
2. S.E. Ziemniak & M. Hanson, Corrosion Science, Vol. 48 (2006) 498-521
3. M. Bojinov, P. Kinnunen, K. Lundgren & G. Wikmark, Characterization and modelling of oxide films on stainless steels and nickel alloys in light water reactors, VTT Research Report BTUO73-041285 (2004).
4. S. Lozano-Perez & J.M. Titchmarsh, Materials at High Temperatures, Vol. 20, No. 4, Nov. 2003, pp. 573-579 (7).
5. L.E. Thomas, L.A. Charlot, S.M. Bruemmer, in New Techniques for Characterizing Corrosion and Stress Corrosion, R.H. Jones and D.R. Baer, Eds., The Minerals, Metals and Materials Society, 175-191 (1996).
6. L. Thomas, B.R. Johnson, J.S. Vetrano & S.M. Bruemmer, Proceedings of the 12th Int. Conf. on Env. Deg. of Mat. in Nuclear Power Syst-Water Reactors, T.R. Allen, P.J. King and L. Nelson, Eds, The Minerals, Metals and Materials Society, 567-577 (2005).
7. H. Hänninen, A. Toivonen, A. Brederholm,T. Saukkonen, U. Ehrnsten and P. Aaltonen, Crack Chemistry of Ni-based Weld Metals in “Doped Steam" Test, ICG-EAC 2009 (confidential).
8. W. Karlsen & P. Aaltonen, in Appendix 7 of Minutes of PERDI 5th Project Board Meeting on 17.6.2008.
9. L. Thomas, J.S. Vetrano S.M. Bruemmer, P. Efsing, B. Forssgren, G. Embring & K. Gott, Proceedings of the 11th Int. Conf. on Env. Deg. of Mat. in Nuclear Power Syst.-Water Reactors, G.S. Was, L. Nelson & P.J. King , Eds., NACE, 1212-1225 (2003).